Food Bioscience 79 (2026) 108811

Contents lists available at ScienceDirect

Food Bioscience

journal homepage: www.elsevier.com/locate/fbio

Visible-light-based antimicrobial strategies for wheat seeds and sprouts: Comparative study of ZnO nanoparticles and a chlorophyllin–chitosan complex

Kristina Aponiene [a,*], Irina Buchovec [a], Gabriele Vasiliauskaite [a], Alisa Gricajeva [b], Pranciskus Vitta [a]

[a] Vilnius University, Faculty of Physics, Institute of Photonics and Nanotechnology, Saulėtekio al. 3, LT-10257, Vilnius, Lithuania
[b] Vilnius University, Life Sciences Center, Institute of Biosciences, Saulėtekio al. 7, LT-10257, Vilnius, Lithuania

ARTICLE INFO

Keywords:
Zinc oxide nanoparticles
Chlorophyllin–chitosan complex
Listeria monocytogenes
Escherichia coli
Photoinactivation
Wheat seeds and sprouts

ABSTRACT

Microbial contamination of cereal grains intended for sprouting poses a significant food safety challenge, as conventional decontamination methods often compromise seed viability and nutritional quality. This study assessed the antimicrobial efficacy and safety of two visible-light-activated systems, zinc oxide nanoparticles (ZnO NPs) and a chlorophyllin–chitosan (Chl–CHS) complex, for wheat seed decontamination. Antibacterial efficacy was tested against *Listeria monocytogenes* and *Escherichia coli in vitro*, while antifungal effectiveness was evaluated against yeast and mold populations naturally occurring on wheat seeds.

Under visible light, ZnO NPs demonstrated rapid, broad-spectrum bactericidal activity, reducing *L. monocytogenes* and *E. coli* by > 3 $\log_{10}$ at light doses of 22 and 30 J/cm^2, respectively. The Chl–CHS complex exhibited strong photodynamic efficacy against *L. monocytogenes*, achieving bactericidal inactivation at a lower light dose (3 J/cm^2; 10 min incubation), while *E. coli* required higher light exposure (45 J/cm^2) and longer incubation (60 min). Fungal populations decreased by 68–75% from the original yeast and mold count of approximately 4 log CFU/g.

Germination tests indicated that neither treatment negatively impacted seed viability or sprouting over a five-day period. Total antioxidant capacity remained unchanged compared to untreated controls, indicating that the nutritional quality was preserved. Electron paramagnetic resonance spectroscopy further validated the treatments' safety, as no increase in integrated radical signals was observed after photoactivation, unlike ionizing radiation, which produced stable free radicals.

In summary, visible-light-driven antimicrobial treatments using ZnO NPs and Chl–CHS complex offer an effective, non-thermal, and seed-safe approach for enhancing the microbiological safety of wheat seeds and sprouts.

1. Introduction

The consumption of fresh green wheat and other cereal sprouts has risen significantly over the past decade, driven by growing consumer interest in functional foods and plant-based nutrition. Sprouted grains are generally considered to be more nutritious than their non-germinated counterparts due to biochemical changes that occur during germination, including enhanced enzymatic activity, increased bioavailability of minerals, and accumulation of bioactive compounds (Benincasa et al., 2019; García et al., 2023). Numerous studies have indicated that wheat sprouts are rich sources of vitamins, phenolic compounds, antioxidants, flavonoids, dietary fiber, and essential amino acids (Gan et al., 2017; Ikram et al., 2021). Additionally, germination is associated with a reduction in antinutritional factors such as phytic acid and tannins (Yılmaz Tuncel et al., 2025). These compositional improvements have been linked to potential health benefits, including improved glycemic response and positive effects on gut health, contributing to the growing popularity of wheat sprouts as ingredients in health-oriented food and beverage products (Gan et al., 2017; Maleki et al., 2023).

* Corresponding author.
E-mail address: kristina.aponiene@ff.vu.lt (K. Aponiene).

https://doi.org/10.1016/j.fbio.2026.108811
Received 26 February 2026; Received in revised form 31 March 2026; Accepted 1 April 2026
Available online 2 April 2026

However, cereal grains, such as wheat, are often contaminated by microbes throughout their growth, harvesting, storage, and distribution, posing a continuous challenge to agricultural productivity and food safety. Wheat seeds are frequently contaminated with various microbial populations, including bacterial pathogens as well as spoilage yeasts, and mycotoxin-producing fungi like *Aspergillus*, *Penicillium*, and *Fusarium*, that can affect food safety and result in seed deterioration, decreased vigor, and lower germination potential (Khapre et al., 2020; Magallanes López & Simsek, 2021; Myoda et al., 2019; Yang et al., 2024). Among bacterial contaminants, *Listeria monocytogenes* and *Escherichia coli* are of particular concern due to their prevalence in the food chain and their association with foodborne outbreaks. Notably, the large 2011 outbreak of Shiga toxin–producing *Escherichia coli* O104:H4 linked to fenugreek sprouts in Europe caused more than 3400 infections and 50 deaths (Buchholz et al., 2011). In addition, *Listeria monocytogenes* contamination has been reported in sprouted products and fresh produce, including outbreaks linked to contaminated sprouts and ready-to-eat vegetables (Garner & Kathariou, 2016). Therefore, these microorganisms were selected as representative Gram-positive and Gram-negative bacteria to evaluate the antimicrobial effectiveness of the investigated treatment.

Conventional decontamination strategies for cereal grains and sprouting seeds include chemical disinfectants (e.g., chlorine-based solutions, organic acids, ozone, peroxyacetic acid, hydrogen peroxide) and physical intervention methods (high pressure, thermal treatments, debranning, ionizing irradiation). While these methods can reduce surface microbial loads, their overall effectiveness is often limited, and they negatively impact safety, cost-effectiveness, and food quality (Benincasa et al., 2019; Yang et al., 2024). Chemical treatments may not fully inactivate pathogenic bacteria, yeasts, and molds. Furthermore, the repeated or intensive application of these chemicals can adversely affect seed viability and germination, diminish the sensory and nutritional quality of resulting sprouts, and pose a potential health risk due to chemical residues. In addition, the use of chemical disinfectants raises concerns about environmental impact and consumer acceptance (Ikram et al., 2021; Yang et al., 2024, 2025). Thermal methods can significantly denature enzymes and gluten proteins, making them generally unsuitable for sprouting seeds, as they may damage the embryo (Schmidt et al., 2019). Ionizing irradiation can effectively control a wide range of microorganisms; however, its use is limited by regulatory restrictions, concerns about consumer acceptance, and potential changes it may introduce to seed quality and biochemical properties (Los et al., 2018; Schmidt et al., 2019). These limitations highlight the need for alternative decontamination technologies that can effectively eliminate microorganisms while preserving the seed functionality and meeting consumer demand for minimally-processed, chemical-free food products.

In this context, light-based antimicrobial approaches, particularly photodynamic and photocatalytic methods, have emerged as promising non-thermal alternatives for microbial control in food and agricultural systems. These technologies rely on the activation of photosensitizing compounds or photocatalysts by visible light to generate reactive oxygen species (ROS) capable of microbial inactivation without requiring high temperatures or chemical additives (Biswas et al., 2022; Wainwright et al., 2017; Wang et al., 2017; Youf et al., 2021). Among inorganic photocatalysts, zinc oxide nanoparticles (ZnO NPs) have attracted considerable interest due to their chemical stability, biocompatibility, low toxicity, and strong ability to generate ROS upon photoactivation (Baig et al., 2025). Numerous studies have shown that ZnO NPs exhibit antimicrobial activity against a wide range of microorganisms, even in the absence of light. Unmodified ZnO NPs have been shown to inhibit both Gram-positive and Gram-negative bacteria, including major foodborne pathogens such as *Listeria monocytogenes*, *Escherichia coli*, and *Salmonella spp.*, as well as spoilage yeasts and mycotoxin-producing molds belonging to genera such as *Aspergillus*, *Penicillium*, and *Fusarium*, which are commonly associated with food deterioration and safety concerns (Kim et al., 2020; Mahamuni-Badiger et al., 2024; Sirelkhatim et al., 2015). Their effectiveness as antimicrobials has been validated in liquid cultures, on solid media, and within food-related contexts, reinforcing their potential for use in food safety, agriculture, and post-harvest protection (Kim et al., 2020; Zare et al., 2022).

In addition to their inherent antimicrobial properties, ZnO NPs exhibit enhanced antimicrobial performance upon light activation. Activated by light, ZnO NPs have demonstrated the ability to quickly inactivate bacteria such as *E. coli*, *L. monocytogenes*, *S. aureus*, and *B. subtilis*, as well as fungal contaminants, achieving bactericidal or fungicidal effects at lower concentrations of NPs or shorter incubation times (Kairyte et al., 2013; Aponiene et al., 2017, 2025; Du et al., 2021; Karabaş et al., 2025; Núñez-Salas et al., 2021; Rezaei et al., 2020; Yang et al., 2023). Due to their broad band gap, ZnO NPs are most efficiently activated by ultraviolet radiation (UV-A or UV-B), which promotes the generation of electron–hole pairs (Jin et al., 2019; Kim et al., 2020; Zare et al., 2022); however, the use of UV light may be unfavorable for practical applications because of its limited penetration depth and possible negative effects on food matrices and biological tissues (Csapó et al., 2019). The activation of ZnO NPs by visible light is feasible and thus more appealing for practical applications. It is possible due to intrinsic states and defect-related features, such as oxygen vacancies and surface defects, which enhance light absorption in the visible spectrum (Puranen et al., 2021). Consequently, visible-light-activated ZnO NPs represent a promising alternative for safer and more application-oriented antimicrobial technologies.

Unlike inorganic photocatalysts, chlorophyllin (Chl) – a water-soluble derivative of natural chlorophyll – functions as a bio-based photosensitizer (PS) with a distinct excitation mechanism. Chl absorbs strongly in the visible light region, including the Soret band (~405 nm) and the Q band (~670 nm), allowing it to be activated efficiently by low-energy visible-light irradiation (Buchovec et al., 2016). Chl is an anionic PS that generates ROS upon light activation; however, its antimicrobial activity may be limited by poor interaction with the cell surface, especially with Gram-negative bacteria, due to the negatively charged outer membrane. When combined with biopolymers like chitosan (CHS), Chl-based systems can form stable complexes with enhanced antimicrobial properties under visible light, while leveraging CHS's biodegradability, biocompatibility, and film-forming properties (Buchovec et al., 2016; Rizzi et al., 2016). CHS is a cationic biopolymer that possesses antimicrobial activity and a strong affinity for negatively charged cells' outer membranes. After complexation with Chl, the Chl–CHS complex acquires a net positive charge, thereby promoting stronger interactions with bacterial membranes. This enhanced interaction improves PS adsorption at the cell surface, and the increased local concentration of Chl enhances the photodynamic effect on bacteria. It has been reported that CHS-based matrices can enhance the stability and PDT performance of several PSs under visible light irradiation (Genovese et al., 2025; Lai et al., 2025; Ni et al., 2024; Shrestha & Kishen, 2012; Wang et al., 2022; Zhou et al., 2021). However, most reported systems are either covalent conjugates or solid-film matrices. In this study, we examine a system based on a non-covalent supramolecular complex formed between sodium magnesium Chl and CHS (Chl-CHS), assembled directly from aqueous media, and evaluate the impact of electrostatic interactions and aggregation on photodynamic efficiency. Previous studies have demonstrated the feasibility of Chl–CHS systems for visible-light-driven antimicrobial applications against selected bacteria and fungi in model food systems (Buchovec et al., 2016, 2017; Luksiene & Buchovec, 2019; Lukseviciute & Luksiene, 2020). These findings support the selection of the Chl–CHS complex as a promising candidate for further evaluation under conditions relevant to cereal seed decontamination.

Despite increasing research interest in photoactivated antimicrobial systems, comparative studies evaluating inorganic photocatalytic NPs and bio-based PS complexes under identical experimental conditions and using non-ionizing visible light sources remain limited. Moreover,

most existing studies primarily focus on antimicrobial efficacy, while systematic evaluations of seed quality parameters – such as germination performance, antioxidant capacity, and free radical formation – are much less common. Since food and sprouting applications require both microbial safety and the preservation of biological functions, an integrated assessment is necessary to determine the practical suitability of photoactivated treatments. In this context, 405 nm visible light is particularly relevant as an activation wavelength. It falls within the visible spectrum and is classified as posing no or low photobiological hazard under controlled exposure conditions (Chen et al., 2023; Leanse et al., 2022), supporting its use in food and agricultural decontamination, especially where UV irradiation is not recommended.

The novelty of the present study lies in the direct comparison of visible-light-activated ZnO NPs and a Chl–CHS complex for the decontamination of wheat seeds, combined with a comprehensive evaluation of seed quality and safety.

Accordingly, the aim of this study was to investigate and compare the antimicrobial activity of ZnO NPs and Chl–CHS complex against *L. monocytogenes*, *E. coli*, and naturally occurring yeasts and molds on wheat seeds under visible-light illumination, while simultaneously assessing their effects on seed germination, total antioxidant capacity, and free radical generation. This approach enables evaluation of these systems as safe, non-chemical, and non-thermal decontamination strategies for cereal grains intended for sprouting or food use.

2. Materials and methods

2.1. Preparation and characterization of ZnO NPs and Chl-CHS complex

A 50% colloidal dispersion of ZnO NPs in water with a nonionic dispersant was purchased from Alfa Aesar (NanoShield, Germany). A stock solution was prepared using 0.9% NaCl (Carl Roth, Germany) and was used immediately. Final NP concentrations were achieved by further dilution in 0.9% NaCl.

The Chl–CHS complex used in this study was prepared using non-copperized chlorophyll sodium salt (magnesium Chl, $C_{34}H_{31}MgN_4Na_3O_6$, Mw = 684.9 g/mol; Carl Roth, Germany) and low-molecular-weight CHS (Aldrich, USA), following the protocol described by Buchovec et al. (2016). A Chl stock solution (0.01%, w/v; 0.146 mM) was prepared in deionized water and added dropwise into a CHS solution (1% (w/w) in 0.18% HCl (Supelco, Germany) under vigorous stirring. The resulting solution had a pH of 2.4 at 20 °C. Detailed preparation parameters and physicochemical characterization are available in the original publication (Buchovec et al., 2016). Prior to each experimental series, the freshly prepared Chl–CHS complex was verified spectrophotometrically by recording its absorption spectrum to confirm the presence of the characteristic Soret and Q bands and to ensure batch-to-batch reproducibility.

UV-Vis absorption spectra of ZnO NPs (0.5 mM) and the Chl–CHS complex containing 0.015 mM Chl and 1 g/L CHS were recorded using a Heλios Gamma spectrophotometer (Thermo Scientific, USA) with a 10.01 mm quartz cuvette. Fluorescence spectra were measured using a PerkinElmer LS-55 fluorescence spectrophotometer (Beaconsfield, UK).

For the ZnO NPs, the fluorescence scan was conducted with the following parameters: excitation wavelength of 375 nm, an emission range of 400-700 nm, an excitation slit of 10 nm, an emission slit of 20 nm, and a scan speed of 200 nm/min.

For the Chl–CHS complex, the fluorescence scan was performed with the following parameters: excitation wavelength of 402 nm, emission range of 600-750 nm, excitation slit of 10 nm, emission slit of 20 nm, and a scan speed of 200 nm/min.

For photostability experiments, the absorption spectra of ZnO NPs (0.5 mM) and a Chl–CHS complex (0.015 mM Chl) were recorded before and after exposure to 405 nm light, using the light-emitting diode (LED)-based system described in section 2.2, with doses ranging from 12.7 to 76 J/cm^2. Each spectrum is the average of three independent replicates.

Scanning electron microscopy (SEM) was used to determine the morphology of ZnO NPs and the Chl–CHS complex. Samples were placed on aluminium stubs, air-dried, and coated with a 15 nm gold layer using a Q150T ES sputter coater (Quorum Technologies Ltd., Lewes, England). Samples were imaged using an Apollo 300 scanning electron microscope (CamScan, Bingham, UK) at an accelerating voltage of 20 kV.

2.2. LED-based light source device for photoactivation of ZnO NPs and Chl-CHS complex

An InGaN LED array (LED Engine, Inc., LZ1-00UA00) was used to construct a light source for photoinactivation of microorganisms. It consisted of an illumination chamber and a supply unit (Fig. 1A). The light-emission maximum was at 405 nm, the distance from the top LEDs to the sample was 6 cm, and the irradiance achieved was 10 mW/cm^2. At 3.5 cm from the bottom of the LEDs to the sample, the irradiance was 11 mW/cm^2 (Fig. 1B).

The illumination dose was calculated as light intensity multiplied by irradiation time. The sample exposure time was adjusted according to the equation:

$$E = Pt, \quad (1)$$

Where E is the energy density (dose) in J/cm^2, P is the irradiance (power density) in W/cm^2, and t is the time in seconds.

2.3. Bacterial cultures and growth conditions

Two food-borne bacterial strains were used: *Listeria monocytogenes* $ATC_{L3}C$ 7644 (provided by the National Veterinary Laboratory of Lithuania) and *Escherichia coli* O157:H7 (obtained from the microbial strain collection of the University of Latvia). All strains were initially maintained on Luria-Bertani Agar (LBA; Liofilchem, Roseto degli Abruzzi, Italy) at 37 °C for 24 h. For inoculum preparation, *L. monocytogenes* and *E. coli* cultures were grown overnight (~16 h) at 37 °C in 20 mL of tryptone soya broth supplemented with 0.6% yeast extract (TSYE; Liofilchem, Roseto degli Abruzzi, Italy) and in 20 mL of LB medium, respectively. Cultures were incubated with agitation at 120 rpm (Environmental Shaker – Incubator ES–20; Biosan, Riga, Latvia) overnight. Cultures were diluted 1:20 in fresh TSYE (for *L. monocytogenes*) and LB (for *E. coli*) to an initial optical density at 540 nm (OD_{540}) of 0.164. Bacterial suspensions were then incubated at 37 °C with shaking (120 rpm) until reaching the mid-logarithmic phase, corresponding to ~1.16×10^9 colony-forming units per mL (CFU/mL) and OD_{540} = 0.9 for *L. monocytogenes,* and ~1×10^8 CFU/mL and OD_{540} = 0.9 for *E. coli*. OD was measured using a Heλios Gamma spectrophotometer (Thermo Fisher Scientific) with 10 mm quartz cuvettes. Bacterial cells were subsequently harvested by centrifugation (10 min, 3420×*g*; Mikro 200, Hettich Zentrifugen, Germany), washed once, and resuspended in 0.9% NaCl to a final concentration of ~1×10^7 CFU/mL for subsequent experiments.

2.4. Inactivation of L. monocytogenes $ATC_{L3}C$ 7644 and E. coli O157:H7 by photoactivated ZnO NPs and Chl-CHS complex

For samples activated by light, 20 mL aliquots of a bacterial suspension (1×10^7 CFU/mL in 0.9% NaCl) containing 0.5 mM ZnO NPs (pH 7.2) or a Chl–CHS complex (0.015 mM Chl) (pH 5.0) were incubated in the dark at 37 °C for durations of 10 to 60 min. Following this, 150 μL aliquots of the bacterial suspension were withdrawn, transferred into sterile flat-bottom wells, and exposed to a light dose of 6.3-76 J/cm^2. Dark toxicity samples were not exposed to light, while control samples included bacterial suspensions in 0.9% NaCl without illumination (dark control) and suspensions illuminated with a light dose of 6.3-76 J/cm^2 in the absence of antimicrobial agents (light control).

The antibacterial effect was evaluated by the spread plate method:

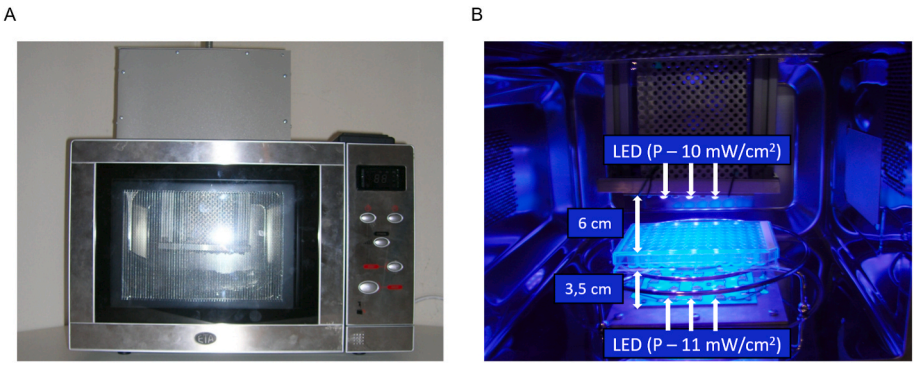

Fig. 1. LED-based light source (A) and its detailed scheme (B).

100 μL of appropriate dilutions of the bacterial test culture after treatment were surface-inoculated onto the LBA plates and incubated at 37 °C for 24 h. The surviving cell population was enumerated and expressed by $\log_{10}$ (CFU/mL). The survivor ratio was determined using the formula $\log_{10}(N/N_0)$, where N represents the CFU/mL in the sample after treatment, and N_0 indicates the initial CFU/mL prior to treatment. Counts of ≤ 1 $\log_{10}$ (CFU/mL) were below the detection limit and were therefore considered undetectable.

2.5. Decontamination of wheat seeds from yeasts and molds by photoactivated ZnO NPs and Chl-CHS complex

The wheat seeds (*Triticum aestivum*) were obtained from local farmers. No chemical treatments were applied to the seeds before the experiments. The seed samples, each consisting of 100 seeds (approximately 5 g), were placed in sterile flasks and soaked in a solution containing 5 mM ZnO NPs or Chl–CHS complex (0.015 mM Chl). The treatment concentration of ZnO NPs was selected based on the antimicrobial levels reported in food-related studies and on preliminary trials conducted in this work to achieve effective microbial inhibition without adversely affecting seed germination. Additionally, the greater resistance of yeasts and molds, due to their complex structures, was considered when determining the concentration range.

The inoculum was incubated in the shaker (130 rev/min) in the dark at 37 °C for 60 min. After incubation, the seed samples were transferred to a sterile Petri dish in the treatment chamber without a cover and exposed to a light dose of 40 J/cm^2. Dark toxicity samples were treated with ZnO NPs or the Chl–CHS complex in the absence of illumination. The control samples were soaked in a 0.9% NaCl solution without subsequent illumination. Illumination alone at a light dose of 40 J/cm^2 had no measurable effect on total yeast and mold counts on wheat seeds (data not shown).

After treatment, each sample was mixed with 45 mL of 0.9% NaCl in a sterile 100 mL BagPage and homogenized for 60 s using a BagMixer (Interscience, France). Next, 100 μL of appropriately diluted homogenized seed suspension was inoculated onto dichloran glycerol (DG18) agar plates (Liofilchem, Italy). Following this, all plates were incubated in a thermostat at 30 °C for 144 h. The surviving cell population was enumerated and expressed as $\log_{10}$ (CFU/g). The growth of micromycetes was expressed as a percentage relative to the untreated control, which was set at 100%. The naturally contaminated wheat seeds used in this study carried an initial yeast and mold population of approximately 4 log CFU/g.

2.6. Wheat germination assay

Control and treated seeds (100 seeds per sample) were germinated on filter paper in Petri dishes in the dark at 25 °C for 5 days, with the filter paper moistened daily. The sprouting of the wheat seeds was assessed daily by counting the number of germinated seeds and expressing this count as a percentage.

2.7. Evaluation of total antioxidant capacity of wheat seeds

The total antioxidant capacity of both treated and untreated seeds was assessed using the ferric reducing ability of plasma (FRAP) method, as described by Benzie and Strain (1996). For the measurement, extracts were prepared by combining 0.5 g of seeds with 25 mL of methanol through homogenization. The FRAP working solution comprised 0.3 M acetate buffer (pH 3.6), 0.01 M 2,4,6-tripyridyl-s-triazine (TPTZ) in 0.04 M HCl, and 0.02 M $FeCl_3{\cdot}6H_2O$ in distilled water. The FRAP reagent was freshly prepared each day by blending 25 mL of acetate buffer, 2.5 mL of TPTZ, and 2.5 mL of $FeCl_3{\cdot}6H_2O$, and heating to 37 °C in a water bath before use. For measuring antioxidant activity, 3 mL of the FRAP reagent was mixed with 100 μL of the sample solution, and the resulting mixture was recorded at 593 nm after 4 min using a Heλios Gamma (Thermo Scientific) spectrophotometer. A standard curve was generated using a solution of Fe (II) sulfate ranging from 100 to 1000 μM. The results were expressed as mM Fe^{2+}/kg of the food material's dry weight.

2.8. Electron paramagnetic resonance measurements

The generation of free radicals both in control and treated wheat seeds was determined by electron paramagnetic resonance (EPR) spectroscopy. The wheat seeds were placed in capillaries (BLAUBRAND micropipettes, intraMark, Hinckley, Great Britain), which were then inserted into standard EPR tubes for measurement. Measurements were performed on a Bruker Elexsys E580 FT-EPR spectrometer (Billerica, USA) operating at X-band. The EPR spectra were recorded at a microwave frequency of 9.85 GHz and a magnetic field modulation frequency of 100 kHz.

To conduct a quantitative comparison, the area under the absorption curves was calculated through double integration of the first-derivative EPR spectra to evaluate differences in radical content across treatments. Ionizing irradiation at a dose of 0.5 kGy was applied as a positive control to generate stable radiation-induced radicals and to confirm the EPR method's effectiveness in detecting persistent paramagnetic species in wheat seeds. All EPR measurements were carried out under consistent instrumental settings, and spectra were baseline-corrected before integration.

The g-factor values were determined based on the EPR resonance condition using the equation:

$$g = \frac{h\nu}{\beta B_0} \tag{2}$$

where h is Planck's constant ($h = 6.626 \times 10^{-34}$ J/s), ν is the microwave frequency (9.85 GHz), β is the Bohr magneton ($9.2740154 \times 10^{-24}$ J/T), and B_0 is the magnetic field strength at the center of the resonance line (mT). The magnetic field position corresponding to the zero-crossing of

the first-derivative EPR spectrum was used to determine B_0.

2.9. Statistics

All experiments were performed in triplicate, and results are expressed as mean ± standard deviation. Statistical analyses were conducted using OriginPro 8.1 software (OriginLab Corporation, USA). Differences among multiple treatment groups were evaluated using one-way analysis of variance (ANOVA), followed by Tukey's honestly significant difference (HSD) post-hoc test for pairwise comparisons. For comparisons between two groups, Student's t-test was applied. Differences were considered statistically significant at $p < 0.05$.

3. Results

3.1. Characterization and photostability of ZnO NPs and Chl–CHS complex

The optical characterization of ZnO NPs (0.5 mM) and the Chl–CHS complex (0.015 mM Chl) showed distinct absorption and fluorescence profiles. ZnO NPs exhibited their characteristic absorbance in the UV region at 375 nm, while the Chl–CHS complex displayed a strong absorption band at 405 nm. The ZnO NPs displayed broad fluorescence emission, peaking at 520 nm, while the Chl–CHS complex showed a strong and well-defined fluorescence spectrum, characterized by pronounced emission peaks within the visible region corresponding to the typical fluorescence behavior of Chl-derived compounds, with the main sharp peak occurring at 650 nm (Fig. 2A).

Fig. 2B shows SEM images of ZnO NPs at a concentration of 0.5 mM, indicating a heterogeneous morphology with irregularly shaped particles and a tendency to form aggregates. The NPs appeared loosely clustered, consistent with the typical behavior of ZnO NPs in saline environments, driven by interparticle interactions. Fig. 2C presents the SEM image of the Chl–CHS complex (0.015 mM Chl), which exhibited a markedly different morphology characterized by a more uniform and continuous surface structure. The matrix appeared relatively smooth with evenly distributed porous or granular features, suggesting the formation of an organized composite structure rather than discrete particulate aggregates. This morphology indicates the successful incorporation or association of chlorophyll within the chitosan-based matrix.

Illumination with increasing doses from 12.7 to 76 J/cm^2 produced measurable changes in the absorbance spectra for both materials, as shown in the corresponding photostability graphs (Fig. 3). The spectra overlap closely, with only gradual, minor shifts observed between the non-illuminated sample and those exposed to progressively higher light doses. Across the series, the overall spectral shapes remain consistent, and the absorbance intensities show slight changes at increasing doses.

3.2. Antibacterial effect of photoactivated ZnO NPs and Chl–CHS complex on L. monocytogenes and E. coli in vitro

The antibacterial tests indicated that the decrease in bacterial levels of *L. monocytogenes* $ATC_{L3}C$ 7644 *and E. coli* O157:H7 was influenced by the duration of incubation (Fig. 4) and the dose of illumination (Fig. 5) following treatment with photoactivated ZnO NPs and the Chl–CHS complex.

Fig. 4 represents the response of bacteria to increasing incubation times when exposed to visible-light-activated ZnO NPs and the Chl–CHS complex. When examining the effects of treatments under dark conditions (without illumination), the data revealed that neither ZnO NPs nor the Chl–CHS complex exhibits significant antibacterial activity against *Listeria* cells in the absence of light (Fig. 4A). However, the ZnO NPs demonstrated a measurable antibacterial effect against *Escherichia*. In the non-illuminated samples containing 0.5 mM ZnO NPs, *Escherichia* counts decreased by 0.5-1.4 log units as incubation time increased from 30 to 60 min (Fig. 4B). This suggests that the NPs exhibit partial antibacterial activity even in the absence of light. In contrast, the Chl-CHS complex shows no significant change compared to the control values for *Escherichia* cells across all incubation periods under dark conditions.

Both treatments required illumination to demonstrate stronger antibacterial activity. Longer incubation periods before illumination led to greater bacterial inactivation; however, the two antimicrobial systems differ significantly in their efficiency.

For both *L. monocytogenes* and *E. coli*, treatment with 0.5 mM ZnO NPs activated with a light dose of 17.3 J/cm^2 resulted in a rapid decline in bacterial viability. This led to a bactericidal reduction of at least 3 log units (99.9%) within relatively short incubation times of 9 min for *L. monocytogenes* and 20 min for *E. coli*. Additionally, *Listeria* showed a slightly faster decline in population than *Escherichia*, suggesting greater susceptibility under these conditions.

The Chl–CHS complex (0.015 mM Chl) effectively reduced the viability of both Gram-positive *Listeria* and Gram-negative *Escherichia*, although its efficacy varied significantly between the two types. The complex was particularly effective against *L. monocytogenes*, achieving its bactericidal reduction threshold more quickly. The minimum pre-illumination incubation time required to achieve a bactericidal effect was only a few minutes (Fig. 4A). In contrast, its effectiveness against *E. coli* was weaker, requiring a longer incubation time of 48 min and

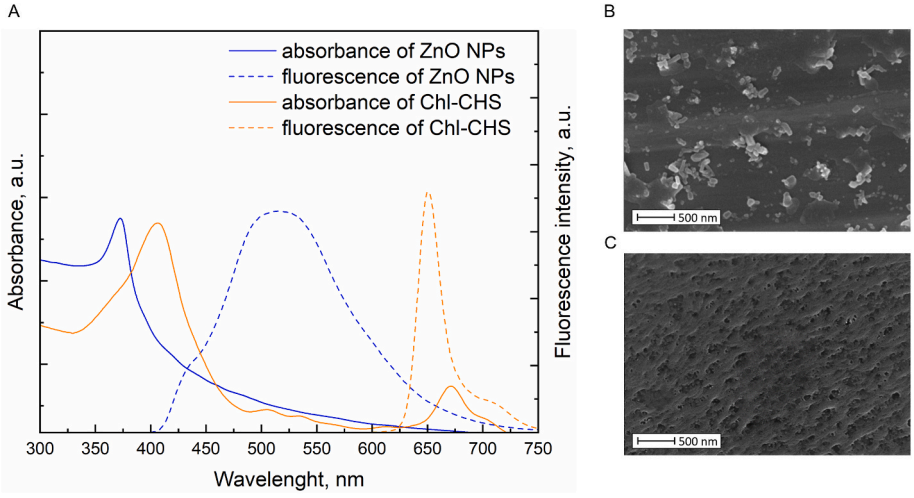

Fig. 2. Optical and structural characterization of ZnO NPs and the Chl–CHS complex in NaCl: (A) absorption and fluorescence spectra; SEM images of (B) ZnO NPs (0.5 mM) and (C) the Chl–CHS complex (0.015 mM Chl).

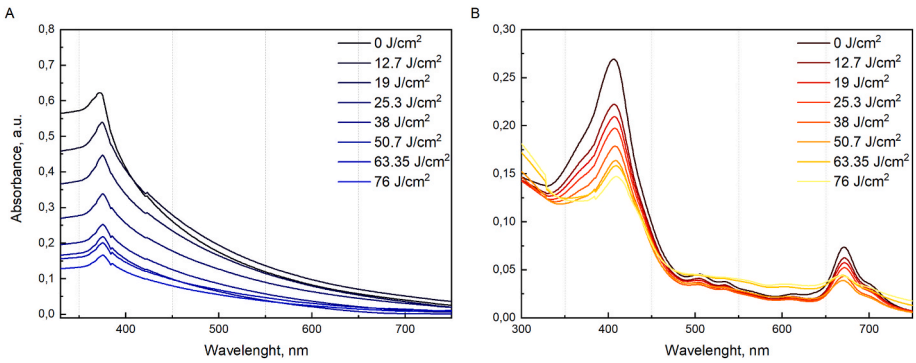

Fig. 3. Absorbance spectra of ZnO NPs (0.5 mM) (A) and Chl–CHS complex (0.015 mM Chl) (B), plotted as a function of illumination dose.

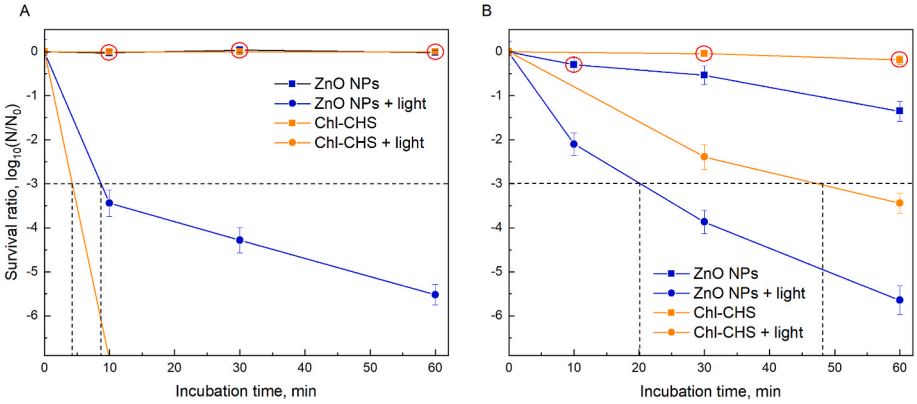

Fig. 4. Inactivation of *L. monocytogenes* $ATC_{L3}C$ 7644 (A) and *E. coli* O157:H7 (B) by photoactivated ZnO NPs (0.5 mM; 17.3 J/cm^2 illumination dose) and Chl–CHS complex (0.015 mM Chl; 38 J/cm^2) as a function of the used incubation time. Each point represents the mean value of 3–6 independent experiments. Error bars are not always visible due to small standard deviations. The dashed black lines indicate the minimum incubation times required to achieve a bactericidal effect ($\geq$3 $\log_{10}$ reduction). Red circles indicate differences that are not statistically significant ($p \geq 0.05$) compared to the control group (0 min incubation; 0 J/cm^2).

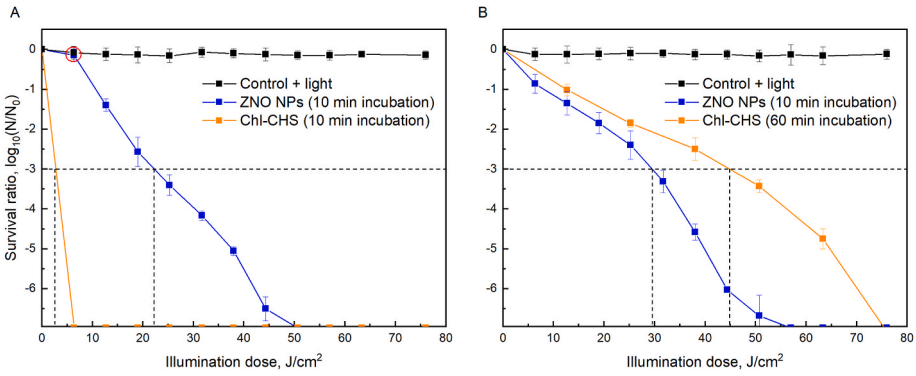

Fig. 5. Inactivation of *L. monocytogenes* $ATC_{L3}C$ 7644 (A) and *E. coli* O157:H7 (B) by photoactivated ZnO NPs (0.5 mM; 10 min incubation) and Chl–CHS complex (0.015 mM Chl; 10 and 60 min incubation) as a function of illumination dose. Each point represents the mean value of 3–6 independent experiments. Error bars are not always visible due to small standard deviations. The dashed black lines indicate the minimum illumination doses required to achieve a bactericidal effect ($\geq$3 $\log_{10}$ reduction). The red circle represents a difference that is statistically insignificant ($p \geq 0.05$) when compared to the light control.

higher illumination levels (38 J/cm^2) to achieve reductions comparable to those with ZnO NPs (Fig. 4B).

The illumination–dose–dependent inactivation curves showed the relationship between light dose and bacterial survival for both treatment systems (Fig. 5). Illumination alone did not affect the viability of either *L. monocytogenes* or *E. coli*, as light-exposed controls showed no measurable reductions in cell counts under any tested dose. However, when ZnO NPs or the Chl–CHS complex were combined with illumination, a dose-dependent decrease in bacterial survival was observed for both microorganisms. Treatment with 0.5 mM ZnO NPs after a 10-min incubation resulted in a bactericidal effect on the *Listeria* culture at an illumination dose of 22 J/cm^2. Meanwhile, the Chl–CHS complex (0.015 mM Chl) was even more effective, requiring only 3 J/cm^2 of illumination after 10 min of incubation to achieve the same reduction in bacterial count. In *E. coli*, bactericidal inactivation was observed only at higher illumination doses. Treatment with 0.5 mM ZnO NPs following a 10-min incubation resulted in a bactericidal reduction at an illumination dose of 30 J/cm^2. Regarding the Chl–CHS complex (0.015 mM Chl), bactericidal activity against *E. coli* necessitated both a longer incubation time (60 min) and a higher illumination dose (45 J/cm^2).

Across both treatments, *L. monocytogenes* showed greater sensitivity than *E. coli*, reaching undetectable levels at lower illumination doses. Specifically, *L. monocytogenes* was inactivated to an undetectable level at 51 J/cm^2 after a 10-min incubation with 0.5 mM ZnO NPs and at 6 J/cm^2 after a 10-min incubation with a Chl–CHS complex (0.015 mM Chl). In contrast, *E. coli* required illumination doses of 57 J/cm^2 and 76 J/cm^2, respectively, to achieve the same level of inactivation under the same experimental conditions with ZnO NPs and the Chl–CHS complex treatments.

3.3. Decontamination of wheat seeds by photoactivated ZnO NPs and Chl–CHS complex

Fig. 6 presents both quantitative and visual results illustrating the decontamination of naturally contaminated wheat seeds treated with photoactivated ZnO NPs (5 mM) and the Chl–CHS complex (0.015 mM Chl).

Illumination alone (40 J/cm^2) did not affect the total yeast and mold population on wheat seeds (data not shown). Additionally, neither ZnO NPs nor the Chl–CHS complex reduced contamination in the absence of illumination. However, when combined with light exposure, both treatments resulted in a significant reduction in yeast and mold levels. Seeds treated with ZnO NPs or a complex of Chl–CHS (incubated for 60 min followed by 40 J/cm^2 of illumination) resulted in a 68-75% decrease in yeast and mold counts compared to untreated controls (Fig. 6). The visual images confirm the decreased surface contamination.

3.4. Germination of wheat seeds after the treatment with photoactivated ZnO NPs and Chl–CHS complex

Fig. 7 presents both the quantitative germination data (panel A) and the visual appearance of wheat sprouts (panel B) after 5 days for control seeds and seeds treated with ZnO NPs or the Chl–CHS complex, either non-photoactivated or activated by visible light.

All three curves exhibited a similar germination pattern. Over the 5-day period, germination rates increased gradually, with treated samples closely matching the control values throughout the measurement period. Neither treatment showed any noticeable differences or delays in germination onset. By day 5, all groups reached high germination rates, with treated seeds overlapping or nearly aligning with the control curve, indicating similar sprouting behavior. Each data point represents the mean of three independent experiments, with 100 seeds per treatment; error bars indicate standard deviations.

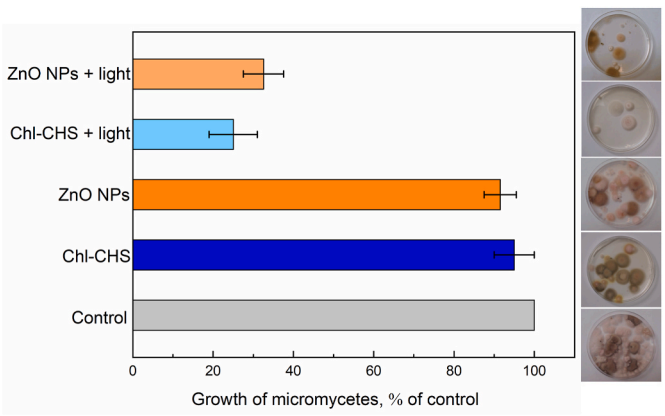

Fig. 6. Decontamination of wheat seeds by photoactivated ZnO NPs (5 mM) and Chl–CHS complex (0.015 mM Chl) (60 min incubation; 40 J/cm^2 light dose): quantitative and visual data. Every point represents the mean of 3–6 independent experiments.

3.5. Evaluation of total antioxidant capability of wheat seeds after the treatment by photoactivated ZnO NPs and Chl–CHS complex

Fig. 8 presents the total antioxidant capacity of wheat seeds treated with photoactivated ZnO NPs and the Chl–CHS complex, as well as non-light-activated treatments, compared with untreated control seeds. The values are expressed as mM Fe^{2+}/kg dry weight, and each bar represents the mean of triplicate measurements.

All groups exhibited FRAP values of similar magnitude. The treated samples are at levels comparable to the control, showing no significant increase or decrease in total antioxidant content. The error bars, which reflect standard error, are included but appear small, suggesting low variability among the replicates.

3.6. Electron paramagnetic resonance signal in wheat seeds after the treatment by photoactivated ZnO NPs and Chl–CHS complex

Electron paramagnetic resonance (EPR) spectra of control wheat seeds and seeds treated with photoactivated ZnO NPs or the Chl–CHS complex are presented in Fig. 9. Both first-derivative and integrated spectra are shown. An additional spectrum of seeds irradiated with 0.5 kGy ionizing radiation is provided for comparison.

The control seeds and those treated with ZnO NPs or Chl-CHS complex exhibited similar first-derivative EPR profiles, characterized by low-intensity signals with comparable line shapes and amplitudes. These spectra closely overlap, indicating minimal differences among the three groups under these conditions. The EPR spectra of wheat seeds treated with photoactivated ZnO NPs or the Chl–CHS complex exhibited a single weak paramagnetic signal centered in the $g \approx 2.00$ region. The calculated g-factor, determined from the resonance magnetic field using the standard resonance condition, was $g = 2.00–2.003$, which is characteristic of carbon- and oxygen-centered organic radicals naturally present in plant matrices (Baltrėnaitė-Gedienė et al., 2022; Vejerano & Ahn, 2023). Importantly, no increase in signal amplitude or emergence of additional spectral components was observed in treated samples compared with untreated controls.

To compare the approved irradiation levels for food applications, EPR measurements were performed on samples irradiated at 0.5 kGy. This dose is significantly below the maximum limit set by the Codex General Standard for Irradiated Foods (Codex General Standard for Irradiated Foods, 2003), which allows for irradiation doses of up to 10 kGy for food-related uses. The spectrum of the sample irradiated at 0.5 kGy shows a significantly stronger, more prominent EPR signal, with a much greater amplitude than those of the other groups. Additionally, the shape and intensity of this spectrum clearly differ from those of the non-irradiated samples. The spectral shape and g-factor value ($g = 2.006$) were consistent with radiation-induced radicals previously assigned to starch-derived hydroxyl and peroxyl species in cereal grains (Korkmaz & Polat, 2000; Vazirov et al., 2023).

To enable a quantitative comparison between treatments, the EPR spectra were converted from first-derivative form to absorption spectra and subsequently double-integrated (Fig. 9b). The integrated spectra show a consistent pattern. The control, ZnO NPs-treated, and Chl-CHS complex-treated seeds display low and closely grouped integrated signal traces, with minimal separation between them. In contrast, the sample irradiated at 0.5 kGy exhibits a significantly higher integrated signal, resulting in a distinct curve that sets it apart from the other three spectra. This indicates a substantially greater magnitude of radical-related signals in the irradiated sample.

4. Discussion

The current investigation presents a comprehensive evaluation of two visible-light-activated antimicrobial systems: ZnO NPs and a Chl–CHS complex. This study examines their effects on wheat seeds, focusing on microbial inactivation, seed germination efficiency,

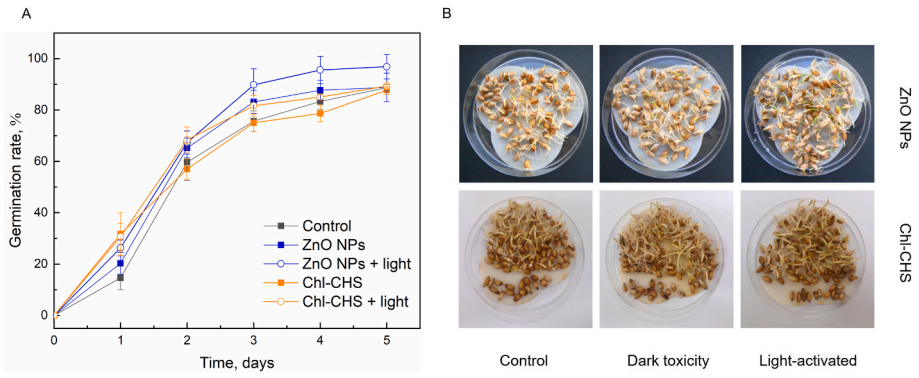

Fig. 7. Sprouting of wheat seeds following treatment with photoactivated ZnO NPs (5 mM) and Chl–CHS complex (0.015 mM Chl) (60 min incubation; 40 J/cm^2 light dose) compared with the control. The results are presented as quantitative germination data (A) and visual observations (B) after 5 days. Each data point represents the mean of three independent experiments, with 100 seeds per treatment. The germination percentage is expressed as the mean number of germinated seeds from the three experiments.

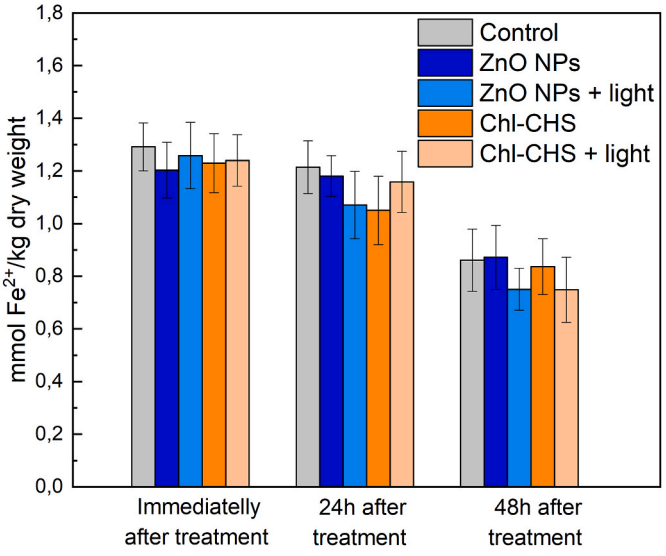

Fig. 8. Total antioxidant capacity in wheat seeds after the treatment with ZnO NPs (5 mM) and Chl–CHS complex (0.015 mM Chl) (60 min incubation; 40 J/cm^2 light dose) compared with the control.

antioxidant potential, and free radical formation. While both systems demonstrated effective light-induced antimicrobial activity, their performance differed in terms of inactivation kinetics, microbial selectivity, and potential applicability in food systems.

The optical analysis of ZnO NPs and the Chl–CHS complex provides important insights into their behavior during photoactivation and their stability upon exposure to visible light, which are directly linked to their effectiveness in antimicrobial applications. The absorption spectra indicated that both systems align well with the 405 nm LED used in this study, enabling a direct comparison of these two systems under the same photoactivation conditions (Fig. 2). ZnO NPs displayed a distinctive absorption edge in the near-ultraviolet region around 375 nm, which is in line with transitions related to the intrinsic band gap, while also permitting excitation by near-visible light due to defect states typically found in nanoscale ZnO (Janotti & Van de Walle, 2009; Singh et al., 2024). In comparison, the Chl–CHS complex exhibited a significant absorption peak at 405 nm, which aligns with the Soret band of Chl, thereby ensuring efficient excitation under the illumination conditions used (Buchovec et al., 2017; Jiang et al., 2024; Li et al., 2017). Fluorescence measurements revealed distinct photophysical characteristics of the two systems. ZnO NPs displayed a broad emission spectrum peaking at 520 nm, indicating radiative recombination associated with defects, which are essential for producing ROS. In contrast, the Chl–CHS complex emitted strongly at 650 nm, a characteristic of chlorophyll derivatives, suggesting that Chl retains its photoactive electronic configuration upon complexation with CHS. The preserved fluorescence emission suggests that Chl remains photoactive within the Chl–CHS complex under the tested conditions, although the occurrence of aggregation-related effects cannot be excluded based solely on steady-state absorption and fluorescence measurements.

SEM provided additional insight into the morphology of the tested materials. ZnO NPs exhibited a heterogeneous structure, with irregularly shaped particles and a tendency to form aggregates, consistent with

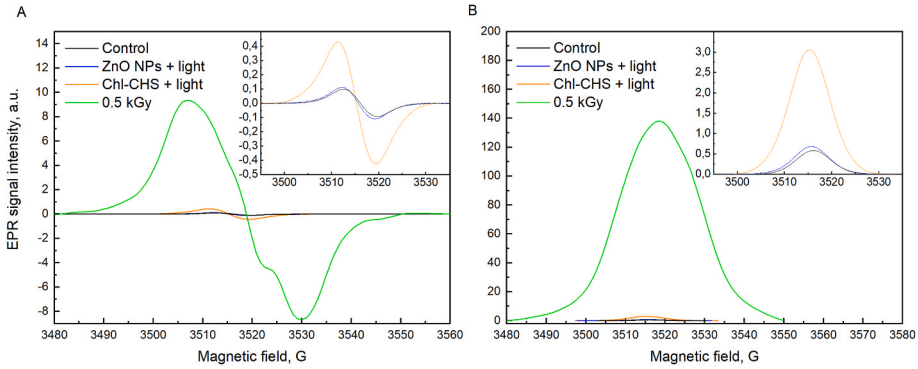

Fig. 9. EPR spectra of wheat seeds after treatment with ZnO NPs (5 mM) and Chl–CHS complex (0.015 mM Chl) (60 min incubation; 40 J/cm^2 light dose) compared with untreated control seeds and seeds subjected to ionizing irradiation at 0.5 kGy. Panel A displays the first derivative of the spectrum, while panel B presents the corresponding integrated signal spectrum.

their high surface energy and behavior in saline media. In contrast, the Chl–CHS complex displayed a more uniform and continuous morphology, characterized by a relatively smooth matrix with dispersed microstructural features. These observations suggest the formation of an organized composite system that may influence interactions with microbial cells and contribute to overall antimicrobial performance.

The physicochemical properties of the ZnO NPs used in this study have been previously characterized in detail (Aponiene et al., 2025). Briefly, at the working concentration of 0.5 mM, dynamic light scattering analysis revealed a particle size distribution ranging from approximately 80 to 400 nm, with an average hydrodynamic diameter of ~190 nm, indicating partial aggregation in saline media. Structural characterization by X-ray diffraction revealed a high-purity hexagonal wurtzite phase, while FTIR analysis confirmed the presence of Zn–O stretching vibrations and surface functional groups associated with adsorbed species (Aponiene et al., 2025).

Photostability studies showed that both ZnO NPs and the Chl–CHS complex did not exhibit significant changes in their spectral profiles when irradiated with increasing doses of visible light up to 76 J/cm^2. Specifically, ZnO NPs gradually lost absorbance intensity without significant changes in the absorption edge position (Fig. 3). This effect can be assigned to previously reported photocatalytic properties of ZnO, where semiconductor properties remain intact during irradiation and surface processes are responsible for ROS generation (Du et al., 2021; Sirelkhatim et al., 2015; Wang et al., 2017). The absence of significant spectral shifts in the present study suggests that no major alterations of the ZnO crystalline structure occurred within the applied light dose range.

Similarly, the Chl–CHS complex maintained its characteristic Soret (~405 nm) and Q (~670 nm) absorption bands during illumination. Earlier studies have described the absorption and fluorescence properties of Chl–CHS systems and confirmed their photoactivity (Buchovec et al., 2016; Luksiene & Buchovec, 2019); however, a systematic evaluation of their stability under increasing visible-light doses has not been reported previously. Our findings demonstrate that the observed decrease in absorbance did not involve shifts in the positions of the major peaks or the development of new absorbance bands, suggesting that no substantial alterations in the electronic configuration of Chl were evident under the applied irradiation conditions. Notably, the observed photostability of the Chl–CHS complex is particularly important, as free chlorophyll derivatives are known to be prone to photodegradation under light exposure (Buchovec et al., 2022; Li et al., 2022; Yi et al., 2023). The interaction with CHS may contribute to the formation of a protective microenvironment that stabilizes the photosensitizer and mitigates photochemical degradation. Overall, both systems demonstrated optical stability under irradiation, ensuring sustained ROS generation for reliable antimicrobial activity. Moreover, photostability is particularly important for practical applications, as it indicates the potential for sustained antimicrobial performance without rapid degradation of the active components, which is a common limitation of many photosensitizing systems.

Results indicated that both ZnO NPs and the Chl–CHS complex require light activation to achieve significant antimicrobial effects, confirming their photocatalytic and photodynamic nature (Figs. 4–5). Illumination alone had no measurable effect on bacterial viability (Fig. 5; control + light samples), which is consistent with previous studies (Buchovec et al., 2010; Kairyte et al., 2013; Kumar et al., 2014). Incubation of bacterial cells with the Chl–CHS complex in the dark for 60 min also showed no antibacterial activity (Fig. 4), indicating that ROS generated under visible light play a central role in microbial inactivation. Previous research supports this conclusion, showing that a longer incubation time – specifically, twice as long (120 min) – is needed to achieve statistically significant inactivation of *Salmonella* cells (Buchovec et al., 2016). In contrast, ZnO NPs demonstrated a modest antibacterial effect against *E. coli*, even without illumination (Fig. 4B). This effect may be attributed to direct interactions between the NPs and the bacterial cells, leading to membrane destabilization, a phenomenon that has been previously reported for metal oxide nanoparticles (Generalova & Dushina, 2025; Mendes et al., 2022; Stankic et al., 2016). Additionally, Lakshmi Prasanna and Vijayaraghavan (2015) demonstrated that the antibacterial activity of ZnO NPs in the dark can be attributed to ROS generated by the interaction of water or moisture with superoxide species, a process facilitated by surface defects. However, a more significant antibacterial effect is observed when the photoactive material is combined with illumination at 405 nm.

Upon photoactivation, ZnO NPs induced rapid inactivation of both *L. monocytogenes* and *E. coli*, resulting in a clear bactericidal effect. This effect was achieved with relatively short exposure times and moderate illumination, indicating high antimicrobial efficiency. Further increases in light exposure enabled complete inactivation of both bacterial populations to undetectable levels, demonstrating a clear dose-dependent response of the photocatalytic system. The rapid response indicates that ZnO NPs function as a high-intensity, broad-spectrum antimicrobial system, particularly suitable for applications requiring fast, efficient decontamination. Earlier studies demonstrated that under visible light ($\lambda > 420$ nm), ZnO NPs markedly reduced *E. coli* viability by over 90% after 6 h at 1.23×10^{-4} M (Yang et al., 2023), while broad-spectrum artificial solar light (300–1000 nm) achieved 6-log inactivation of *E. coli* and 1-log reduction of *Enterococcus sp.* (Núñez-Salas et al., 2021). Other studies using UVA, UV–visible, or UV wavelengths (Ann et al., 2014; Du et al., 2021; Karabaş et al., 2025; Rezaei et al., 2020) reported antimicrobial effects as well, but these conditions do not isolate visible-light activation, and in some cases, visible or longer wavelengths (e.g., 500 nm) had no effect on microbial proliferation.

The Chl–CHS complex displayed a distinct antimicrobial profile, demonstrating particularly strong effectiveness against *L. monocytogenes* at very low illumination doses, whereas higher illumination doses and extended incubation times were required to achieve similar reductions in *E. coli* (Figs. 4–5). As illustrated in Fig. 4, the Chl–CHS complex showed notably strong activity against *L. monocytogenes*, achieving a bactericidal reduction after only a brief incubation period prior to illumination. In contrast, *E. coli* required significantly longer incubation times, reaching the bactericidal threshold only after approximately 48 min of pre-incubation at higher illumination doses, indicating that the Gram-negative bacterium is less susceptible to this photodynamic system. This behavior suggests that photodynamic inactivation is more dependent on interaction time and cell surface accessibility, making it sensitive to structural differences in bacterial cell envelopes.

The illumination dose–response behavior further supports the distinct susceptibility patterns of the two bacteria toward the Chl–CHS system (Fig. 5). After a 10-min incubation with Chl–CHS complex (0.015 mM Chl), *L. monocytogenes* was reduced to a bactericidal level with a light dose as low as 3 J/cm^2 and achieved inactivation to an undetectable level at 6 J/cm^2. In contrast, *E. coli* exhibited markedly higher resistance, requiring illumination doses of up to 45 J/cm^2 for bactericidal reduction and 76 J/cm^2 to reach inactivation below the detection limit, even after extended incubation. The differences observed in the antibacterial properties of photoactivated ZnO NPs and the Chl–CHS complex likely arise from the distinct modes of action and their interactions with bacterial cell structures.

Visible-light-activated ZnO NPs exhibit broad-spectrum antimicrobial activity against both Gram-positive and Gram-negative bacteria, attributed to multiple mechanisms of bactericidal action. Upon illumination, NPs act as photocatalysts by absorbing photons with sufficient energy to promote electrons from the valence band to the conduction band, generating electron–hole pairs. These charge carriers participate in redox reactions at the nanoparticle surface, leading to the formation of ROS – primarily superoxide anions ($\cdot O_2^-$), hydroxyl radicals ($\cdot HO$), and hydrogen peroxide (H_2O_2) in the surrounding aqueous environment (Du et al., 2021; Takhar & Singh, 2025), which create significant oxidative stress in microbial cells, resulting in lipid peroxidation of cell membranes, protein oxidation, disruption of cellular enzymatic

functions, and damage to nucleic acids (Fekrirad et al., 2026; Singh et al., 2020). Moreover, ZnO NPs can physically disrupt cell membranes through adhesion and release of Zn^{2+} ions, which interfere with essential cellular processes, such as membrane stability, protein activity, and DNA replication (Vagena et al., 2024; Vitasovic et al., 2024). The synergy of these mechanisms enhances the range of cellular targets and reduces the likelihood that a single bacterial defense mechanism can fully protect the cell, thereby aiding the effective elimination of both bacterial types.

In contrast, the antimicrobial activity of the Chl–CHS complex primarily relies on a photodynamic mechanism. Chl acts as a PS, absorbing visible light and transitioning from its ground state to an excited singlet state, followed by intersystem crossing to a long-lived triplet state. This excited triplet Chl can interact directly with surrounding biological molecules to form ROS such as $\cdot O_2^-$ and ·HO (type I reactions; electron transfer), or, more commonly, it can transfer energy directly to molecular oxygen, resulting in the formation of singlet oxygen ($^1O_2$) (type II reactions; energy transfer), a highly reactive but transient species that can oxidize cellular components close to the PS (Pablos et al., 2024; Zhao et al., 2025). Incorporating CHS into the Chl–CHS complex enhances its antimicrobial activity. The positively charged biopolymer CHS interacts with the negatively charged surfaces of microbial cells through electrostatic forces, promoting close contact between the PS and the target cells (Shrestha & Kishen, 2012). Unlike photocatalytic systems, which depend on semiconductor band structure, photodynamic action relies on the efficient association of the PS with the cell and the localized generation of ROS (Pablos et al., 2024; Zhao et al., 2025). Singlet oxygen, in particular, is considered highly effective against Gram-positive bacteria due to their thick but porous peptidoglycan layer that permits ROS penetration, whereas Gram-negative bacteria have an outer membrane composed of lipopolysaccharides, lipoproteins, and phospholipids, which creates a complex protective barrier (Maldonado-Carmona et al., 2022). Although ROS scavenging experiments were not included in the present study, the proposed photochemical pathways are consistent with the optical properties of the tested systems and with previously reported mechanisms for photoactivated ZnO NPs and Chl-based antimicrobial systems.

These distinct mechanisms underscore the complementary roles of ZnO NPs and PS-based systems, suggesting that application strategies should be customized to target specific pathogens. Visible-light-activated ZnO NPs are promising for inactivation of broad-spectrum microorganisms, while Chl–CHS systems may be especially effective for rapid, targeted control of Gram-positive pathogens under relatively low illumination doses. Overall, the choice of system should be tailored to specific application requirements, including target microorganisms, processing time constraints, and acceptable energy input.

After conducting *in vitro* antibacterial tests, the efficacy of photoactivated ZnO NPs and the Chl–CHS complex was subsequently evaluated against naturally occurring yeasts and molds on wheat grains, which are among the most common sources of microbial contamination in cereal-based foods and sprouting systems and pose a significant risk during storage and sprouting.

Both photoactivated systems successfully reduced the levels of naturally occurring yeasts and molds on wheat seeds, whereas neither light exposure alone nor dark treatment resulted in any notable decontamination (Fig. 6). This suggests that the observed reductions are due to photoinduced antimicrobial effects rather than mechanical washing or mere light exposure. The reduction in yeast and mold counts achieved by this method ranges from approximately 68% to 75%. Although the observed reduction does not correspond to complete sterilization, it is highly relevant for food applications, where partial microbial reduction combined with preservation of seed viability is often preferable to aggressive chemical or thermal treatments. This level of effectiveness is comparable to some conventional decontamination methods applied to cereal grains, which often exhibit limited effectiveness and can negatively impact seed quality.

For example, conventional heat treatments, such as hot-air drying, can reduce fungal contaminants on cereal grains, but this typically requires high temperatures or prolonged exposure. For instance, using superheated steam at 110-200 °C can inactivate molds by approximately 3 logs on wheat kernels within 30 s (Hu et al., 2016). In contrast, conventional steam at 82 °C should be applied for 60 min to reduce the total microbial load on corn grain by about 4 logs (Rose et al., 2012). However, it should be noted that significant loss of seed viability can occur after prolonged treatment with dry heat at 90 °C (Gilbert et al., 2005).

Chemical treatments, such as organic acids and synthetic fungicides, effectively control fungal growth in stored grains, typically reducing it by 1–3 $\log_{10}$ units with increasing dose and exposure time. However, their limited effectiveness, potential for fungal resistance, chemical residues, increasing regulatory restrictions, and rising consumer demand for clean-label products pose challenges (Szczygieł et al., 2024).

Traditional UVC treatment (254 nm) resulted in around 0.42 $\log_{10}$ (~62%) reductions of *F. graminearum* (Popović et al., 2018) at a dose of 1000 mJ/cm^2 and 1.35 $\log_{10}$ (~95%) reductions of *A. flavus* (Udovicki et al., 2022) at 3240 mJ/cm^2 on actual grain kernels, although direct exposure to 254 nm UVC poses significant risks to human skin and eyes, requiring strict shielding and safety measures during application (Jin & Wang, 2024). Pulsed light treatments can achieve significantly greater microbial reductions than standard continuous light sources; for instance, a treatment with a pulsed light delivering 51.2 J/g of total fluence resulted in about a 4 $\log_{10}$ (~99.99 %) decrease in naturally present molds on wheat grain. However, this high level of inactivation was accompanied by an approximate 14–15% reduction in seed sprouting, underscoring the potential effects on seed viability at elevated pulsed-light exposures (Aron Maftei et al., 2014). Ozone fumigation of cereal grains shows varying degrees of antifungal effectiveness, depending on treatment intensity. For instance, treating stored maize with 50 ppm ozone for 3 days results in approximately a 63% reduction in *Aspergillus parasiticus* (Jian et al., 2013). In contrast, higher concentrations or longer exposure times, such as 100 ppm for 6 h in wheat, lead to a roughly 81.6% overall reduction in fungal presence (Sanchez et al., 2025). Additionally, a 24-h exposure to malting barley resulted in reductions of about 99.2% in total fungal count and 98.2% in *Fusarium* incidence (Sanchez et al., 2025). This underscores that effective ozone treatment for decontamination typically requires extended exposure periods or higher concentrations, which could affect grain quality.

From a regulatory perspective, it should be noted that safety criteria for sprouts in the European Union are defined primarily by the absence of specific foodborne pathogens rather than by reductions in total fungal or yeast populations. Commission Regulation (EC) No 2073/2005, as amended by Regulation (EU) No 209/2013, requires the absence of *Salmonell*a and Shiga toxin–producing *Escherichia coli* in sprouts, while additional regulations governing sprouting seeds emphasize hygiene controls and traceability (European Commission, 2005, 2013a; 2013b; 2013c). Therefore, although the treatments evaluated in this study reduced micromycete growth by approximately 68–75% relative to the control, this reduction should be interpreted as evidence of antifungal activity rather than as a direct indicator of compliance with regulatory safety criteria for seeds intended for sprouting.

The ability of ZnO NPs and the Chl–CHS complex to eliminate yeasts and molds is particularly significant for sprouting processes, as they not only cause spoilage but can also produce mycotoxins during the germination phase (Deligeorgakis et al., 2023). The current results suggest that treatments using visible light could improve the microbiological safety of sprouts without the need for chemical fungicides or aggressive physical methods. Additionally, germination tests further validated their suitability for sprouting seeds, as neither photoactivated ZnO NPs nor the Chl–CHS complex negatively affected seed viability, vigor, or sprouting rates (Fig. 7). Treated seeds displayed germination patterns that closely matched those of untreated controls over the 5-day observation period, indicating that no detectable impairment of seed

physiological performance occurred under the applied conditions.

These findings contrast with several reports on traditional chemical and thermal decontamination methods, which have been associated with reduced germination rates or delayed sprouting due to embryo damage, enzyme denaturation, or chemical toxicity. For example, Clear et al. (2002) observed that applying dry heat for 10 days at 80 °C, while effective against *F. graminearum*, significantly diminished the germination rates of both wheat and barley seeds (effects of heat stress); dry heat treatments on seeds at temperatures of 80 °C and above drastically lowered germination percentages compared to the control group, indicating disruption caused by heat to membranes and metabolic processes (Bennett & Colyer, 2010); pulsed light sterilization has been demonstrated to reduce germination rates of seeds intended for sprouting when used at elevated fluences, implying photodamage that goes beyond merely inactivating microbes (Aron Maftei et al., 2014); conventional chlorine-based chemical disinfectants that lowered fungal levels on sprouting seeds also showed links to reduced germination under specific conditions, reflecting the effects of chemical toxicity at greater doses (Shabana et al., 2021).

The preservation of germination performance demonstrated here supports the suitability of photoactivated antimicrobial methods for cereal grains meant for sprouting. Furthermore, the FRAP assay indicated no significant differences in total antioxidant capacity between treated and untreated seeds (Fig. 8), suggesting that neither ZnO NPs nor the Chl–CHS complex altered the overall antioxidant capacity of wheat seeds under the applied conditions. This is particularly relevant, as germinated grains are appreciated for their high antioxidant levels, which enhance their functional and health-promoting properties (Ikram et al., 2021; Sun & Lee, 2025).

Prior research has indicated that various physical and chemical treatments can degrade phenolic compounds or disrupt antioxidant enzymes, thereby reducing the nutritional quality of sprouts. For instance, thermal processing methods such as autoclaving and other heat treatments change the phenolic profiles and antioxidant activity in grain sprouts and seedlings, likely due to phenolic oxidation or polymerization (Randhir et al., 2008). Additionally, ozone treatment has been shown to significantly reduce phenolic content and, consequently, antioxidant potential in both seeds and sprouts. In a study on O_3 exposure at 50 ppm, wheat sprouts showed an 18.0% reduction in total phenolic content compared to untreated controls, while broccoli and radish sprouts experienced decreases of 47.7% and 20.2%, respectively, suggesting that high ozone levels can reduce important antioxidant compounds (Bernate et al., 2024). Furthermore, prolonged UV-C exposure can lead to a decline in phenolic content and antioxidant activity in seeds, due to membrane damage and oxidation (Arcos-Limiñana et al., 2025; Bang et al., 2021; Kamel et al., 2022).

Based on the observation that photoactivated ZnO NPs and the Chl–CHS complex maintained total antioxidant capacity, further examinations of potential oxidative effects at a molecular level were conducted. EPR spectroscopy was used to determine whether these treatments could generate persistent free radicals within the seed matrix, providing an additional safety assessment beyond conventional antioxidant tests. The first derivative EPR spectra from seeds treated with light-activated ZnO NPs or the Chl–CHS complex were highly similar to those of the untreated controls, suggesting no detectable increase in persistent free radical levels (Fig. 9). Conversely, seeds exposed to ionizing radiation (0.5 kGy) displayed a significantly stronger EPR signal, indicating the formation of stable radiation-induced radicals, consistent with earlier findings. For instance, wheat seeds exposed to a low-energy electron beam showed dose-dependent increases in EPR signal intensity over the 0–20 kGy range, with significant radical accumulation detectable even 23 days after irradiation (Vazirov et al., 2023). Rice seeds irradiated with doses of 0.5-5 kGy formed various radical species, identified as hydroxyalkyl (I), aldehydalkyl (II), and an unidentified species (III), with a linear relationship to dose (Polat & Korkmaz, 2003). Horse chestnut seeds exhibited increased EPR signals at doses of 1-10 kGy, with free radicals remaining detectable over time. Notably, samples treated with 5 and 10 kGy still showed radicals 250 days later (Mladenova et al., 2025).

To ensure reliable signal quantification, the first-derivative EPR spectra were double-integrated, thereby eliminating the effects of linewidth, modulation parameters, and overlapping spectral features. This is particularly important in complex biological samples, where multiple radical types may exist within a narrow g-factor range. As shown by Vazirov et al. (2023), the area under the absorption curve, after double integration, is directly proportional to the total amount of paramagnetic centers. Therefore, it serves as the most dependable measure for comparing radical levels across various treatments. The absence of an increase in integrated EPR intensity following photoactivation suggests that the ROS generated during illumination were short-lived and did not result in detectable accumulation of stable radicals within the seed matrix (Victória et al., 2022). This behavior differs from treatment with electron-beam or γ-irradiation, where stable radicals can be detected for weeks and are commonly used as markers of radiation exposure (Mladenova et al., 2025; Vazirov et al., 2023).

These findings are particularly relevant for food safety and regulatory considerations, as concerns about radical formation and the long-term oxidative effects have hindered the acceptance of ionizing irradiation for decontaminating seeds and food. The lack of increased radical signals after visible-light-activated treatments supports the idea that the reactive species produced during illumination are short-lived and restricted to the treatment period, without causing lasting oxidative damage to the seed matrix.

From a practical perspective, these results indicate that visible-light-activated antimicrobial systems could be integrated into seed sanitation and sprout production processes as non-thermal alternatives to traditional disinfectants. Possible applications include pre-germination seed treatment, LED-based decontamination chambers, and clean-label or organic food processing systems. The use of 405 nm visible light is especially advantageous, as it enables effective microbial control while maintaining seed germination capacity, physiological quality, and nutritional properties, making these systems suitable for functional foods like sprouts and microgreens. For such applications, ZnO NPs might be preferred if broad-spectrum activity is desired. In contrast, the Chl–CHS complex may represent a more bio-based alternative for applications aligned with clean-label, sustainability-oriented processing strategies.

Despite the promising findings, several limitations should be acknowledged. First, all experiments were conducted at the laboratory scale using a custom-built visible-light reactor; therefore, further research is required to evaluate the scalability of these systems for seed treatment in larger, industrial settings. Second, the microbiological assessment was limited to two bacterial strains and naturally occurring yeasts and molds, and thus, additional studies involving a broader range of food-relevant pathogens, including spores and biofilm-forming microorganisms, are necessary to expand applicability. Third, although the proposed photochemical mechanisms are supported by optical characterization and existing literature, direct ROS-scavenging experiments were not performed and therefore require further validation. In addition, a more comprehensive evaluation of antioxidant properties using established quantitative assays (e.g., DPPH and ABTS), along with detailed analysis of ROS generation and scavenging, is needed to better elucidate the underlying mechanisms of action. Safety assessment also remains essential, and future studies should address cytotoxicity toward mammalian cells, potential environmental impacts, and dose-dependent effects to ensure safe application. Finally, further work should focus on optimizing treatment parameters for different cereal types, improving process efficiency, and evaluating economic feasibility, scalability, and integration into existing food production systems under realistic processing conditions.

5. Conclusions

In summary, the findings suggest that both ZnO NPs and the Chl–CHS complex act as effective visible-light-based antimicrobial systems, each possessing unique yet complementary properties. ZnO NPs exhibit broad antimicrobial activity and relatively rapid inactivation rates, while the Chl–CHS complex represents a bio-based alternative method with high efficacy against Gram-positive bacteria, which may align well with current clean-label and sustainability-oriented trends.

Importantly, the applied photoactivated treatments preserved seed quality parameters essential for sprouting applications. Neither ZnO NPs nor the Chl–CHS complex adversely affected germination capacity, sprouting kinetics, or seed vigor, and no changes in total antioxidant capacity were detected, indicating maintenance of the nutritional and functional properties of wheat seeds under the tested conditions. In addition, EPR spectroscopy further supported the safety of the photoactivated approaches by demonstrating no detectable accumulation of persistent free radicals.

The comparative evaluation conducted in this research fills a crucial gap in the existing literature, as many earlier studies have focused solely on either inorganic photocatalysts or organic PSs, often without simultaneously assessing seed quality parameters. By combining microbiological effectiveness with physiological and biochemical safety indicators, this study offers a comprehensive approach to assessing visible-light-activated decontamination strategies for cereal grains.

CRediT authorship contribution statement

Kristina Aponiene: Writing – review & editing, Writing – original draft, Visualization, Validation, Methodology, Investigation, Formal analysis, Data curation. **Irina Buchovec:** Writing – review & editing, Validation, Methodology, Investigation, Formal analysis, Data curation. **Gabriele Vasiliauskaite:** Visualization, Formal analysis. **Alisa Gricajeva:** Writing – review & editing, Supervision. **Pranciskus Vitta:** Supervision.

Declaration of competing interest

The authors declare that they have no known competing financial interests or personal relationships that could have appeared to influence the work reported in this paper.

6. Abbreviations

CFU	colony-forming units
Chl–CHS	chlorophyllin–chitosan complex
EPR	electron paramagnetic resonance
FRAP	ferric-reducing ability of plasma
LED	light-emitting diode
LBA	Luria-Bertani Agar
OD_{540}	optical density at 540 nm
PS	photosensitizer
ROS	reactive oxygen species
SEM	scanning electron microscopy
TPTZ	2,4,6-tripyridyl-s-triazine
TSYE	tryptone soya medium supplemented with 0.6% yeast extract
ZnO	NPs zinc oxide nanoparticles

Data availability

Data will be made available on request.

References

Ann, L., Mahmud, S., Bakhori, S. K. M., Sirelkhatim, A., Mohamad, D., Hasan, H., & Seeni, A. (2014). Effect of surface modification and UVA photoactivation on antibacterial bioactivity of zinc oxide powder. *Applied Surface Science, 292*, 405–412. https://doi.org/10.1016/j.apsusc.2013.11.152

Aponiene, K., Gricajeva, A., Zarkov, A., Dobuzinskas, R., & Vitta, P. (2025). Evaluation of visible-light-activated ZnO nanoparticles for sustainable postharvest protection of strawberries. *Food Control.* , Article 111935. https://doi.org/10.1016/j.foodcont.2025.111935

Aponiene, K., Serevičius, T., Luksiene, Z., & Juršėnas, S. (2017). Inactivation of bacterial biofilms using visible-light-activated unmodified ZnO nanorods. *Nanotechnology, 28*(36), Article 365701. https://doi.org/10.1088/1361-6528/aa7a53

Arcos-Limiñana, V., Maestre-Pérez, S., & Prats-Moya, M. S. (2025). A comprehensive review on ultraviolet disinfection of spices and culinary seeds and its effect on quality. *Comprehensive Reviews in Food Science and Food Safety, 24*(1), Article e70076. https://doi.org/10.1111/1541-4337.70076

Aron Maftei, N., Ramos-Villarroel, A. Y., Nicolau, A. I., Martín-Belloso, O., & Soliva-Fortuny, R. (2014). Pulsed light inactivation of naturally occurring moulds on wheat grain. *Journal of the Science of Food and Agriculture, 94*(4), 721–726. https://doi.org/10.1002/jsfa.6324

Baig, A., Siddique, M., & Panchal, S. (2025). A review of visible-light-active zinc oxide photocatalysts for environmental application. *Catalysts, 15*(2), 100. https://doi.org/10.3390/catal15020100

Baltrėnaitė-Gedienė, E., Lomnicki, S., & Guo, C. (2022). Impact of biochar, fertilizers and cultivation type on environmentally persistent free radicals in agricultural soil. *Environmental Technology & Innovation, 28*, Article 102755. https://doi.org/10.1016/j.eti.2022.102755

Bang, I. H., In, J., & Min, S. C. (2021). Inactivation of salmonella on black peppercorns using an integrated ultraviolet-C and cold plasma intervention. *Food Control, 119*, Article 107498. https://doi.org/10.1016/j.foodcont.2020.107498

Benincasa, P., Falcinelli, B., Lutts, S., Stagnari, F., & Galieni, A. (2019). Sprouted grains: A comprehensive review. *Nutrients, 11*(2), 421. https://doi.org/10.3390/nu11020421

Bennett, R. S., & Colyer, P. D. (2010). Dry heat and hot water treatments for disinfesting cottonseed of Fusarium oxysporum f. sp. vasinfectum. *Plant Disease, 94*(12), 1469–1475. https://doi.org/10.1094/pdis-01-10-0052

Benzie, I. F., & Strain, J. J. (1996). The ferric reducing ability of plasma (FRAP) as a measure of "antioxidant power": The FRAP assay. *Analytical Biochemistry, 239*(1), 70–76. https://doi.org/10.1006/abio.1996.0292

Bernate, I., Kince, T., Radenkovs, V., Juhnevica-Radenkova, K., Cinkmanis, I., Bruveris, J., & Sabovics, M. (2024). Impact of ozone exposure on the biochemical composition of wheat, broccoli, alfalfa, and radish seeds during germination. *Agronomy, 14*(11), 2571. https://doi.org/10.3390/agronomy14112571

Biswas, R., Alam, M., Sarkar, A., Haque, M. I., Hasan, M. M., & Hoque, M. (2022). Application of nanotechnology in food: Processing, preservation, packaging and safety assessment. *Heliyon, 8*(11), Article e11795. https://doi.org/10.1016/j.heliyon.2022.e11795

Buchholz, U., Bernard, H., Werber, D., Böhmer, M. M., Remschmidt, C., Wilking, H., … Kühne, M. (2011). German outbreak of *Escherichia coli* O104: H4 associated with sprouts. *New England Journal of Medicine, 365*(19), 1763–1770. https://doi.org/10.1056/nejmoa1106482

Buchovec, I., Klimkaitė, L., Sužiedėlienė, E., & Bagdonas, S. (2022). Inactivation of opportunistic pathogens *Acinetobacter baumannii* and *Stenotrophomonas maltophilia* by antimicrobial photodynamic therapy. *Microorganisms, 10*(3), 506. https://doi.org/10.3390/microorganisms10030506

Buchovec, I., Lukseviciūtė, V., Kokstaite, R., Labeikyte, D., Kaziukonyte, L., & Luksiene, Z. (2017). Inactivation of Gram (−) bacteria Salmonella enterica by chlorophyllin-based photosensitization: Mechanism of action and new strategies to enhance the inactivation efficiency. *Journal of Photochemistry and Photobiology B: Biology, 172*, 1–10. https://doi.org/10.1016/j.jphotobiol.2017.05.008

Buchovec, I., Lukseviciute, V., Marsalka, A., Reklaitis, I., & Luksiene, Z. (2016). Effective photosensitization-based inactivation of Gram (−) food pathogens and molds using the chlorophyllin—Chitosan complex: Towards photoactive edible coatings to preserve strawberries. *Photochemical & Photobiological Sciences, 15*(4), 506–516. https://doi.org/10.1039/c5pp00376h

Buchovec, I., Paskeviciute, E., & Luksiene, Z. (2010). Photosensitization-based inactivation of food pathogen Listeria monocytogenes in vitro and on the surface of packaging material. *Journal of Photochemistry and Photobiology B: Biology, 99*(1), 9–14. https://doi.org/10.1016/j.jphotobiol.2010.01.007

Chen, H., Cheng, Y., & Moraru, C. I. (2023). Blue 405 nm LED light effectively inactivates bacterial pathogens on substrates and packaging materials used in food processing. *Scientific Reports, 13*(1), Article 15472. https://doi.org/10.1038/s41598-023-42347-z

Clear, R. M., Patrick, S. K., Wallis, R., & Turkington, T. K. (2002). Effect of dry heat treatment on seed-borne Fusarium graminearum and other cereal pathogens. *Canadian Journal of Plant Pathology, 24*(4), 489–498. https://doi.org/10.1080/07060660209507038

Codex general standard for irradiated foods (2003) STAN 106-1983, Rev 1-2003. https://www.fao.org/fao-who-codexalimentarius/sh-proxy/ar/?lnk=1&url=https%253A%252F%252Fworkspace.fao.org%252Fsites%252Fcodex%252FStandards%252FCXS%2B106-1983%252FCXS_106e.pdf. Accessed February 20, 2026.

Csapó, J., Prokisch, J., Albert, C., & Sipos, P. (2019). Effect of UV light on food quality and safety. *Acta Universitatis Sapientiae, Alimentaria, 12*(1), 21–41. https://doi.org/10.2478/ausal-2019-0002

Deligeorgakis, C., Magro, C., Skendi, A., Gebrehiwot, H. H., Valdramidis, V., & Papageorgiou, M. (2023). Fungal and toxin contaminants in cereal grains and flours: Systematic review and meta-analysis. *Foods, 12*(23), 4328. https://doi.org/10.3390/foods12234328

Du, M., Zhao, W., Ma, R., Xu, H., Shan, C., Liu, K., … Jiao, Z. (2021). Visible-light-driven photocatalytic inactivation of S. aureus in aqueous environment by hydrophilic zinc oxide (ZnO) nanoparticles based on the interfacial electron transfer in S. aureus/ZnO composites. *Journal of Hazardous Materials, 418*, Article 126013. https://doi.org/10.1016/j.jhazmat.2021.126013

European Commission. (2005). Commission regulation (EC) no 2073/2005 of 15 November 2005 on microbiological criteria for foodstuffs (as amended). *Official Journal of the European Union L, 338*, 1–26. https://eur-lex.europa.eu/legal-content/EN/TXT/?uri=CELEX%3A32005R2073. (Accessed 12 March 2026).

European Commission. (2013a). Commission regulation (EU) no 208/2013 of 11 march 2013 on traceability requirements for sprouts and seeds intended for the production of sprouts. *Official Journal of the European Union L, 68*, 4–6. https://eur-lex.europa.eu/legal-content/EN/TXT/?uri=CELEX%3A32013R0208. (Accessed 12 March 2026).

European Commission. (2013b). Commission regulation (EU) no 209/2013 of 11 march 2013 amending regulation (EC) no 2073/2005 regarding microbiological criteria for sprouts. *Official Journal of the European Union L, 68*, 1–3. https://eur-lex.europa.eu/legal-content/EN/TXT/?uri=CELEX%3A32013R0209. (Accessed 12 March 2026).

European Commission. (2013c). Commission regulation (EU) no 210/2013 of 11 march 2013 on the approval of establishments producing sprouts pursuant to regulation (EC) no 852/2004. *Official Journal of the European Union L, 68*, 7–10. https://eur-lex.europa.eu/legal-content/EN/TXT/?uri=CELEX%3A32013R0210. (Accessed 12 March 2026).

Fekrirad, Z., Darbouy, M., & Molabashi, Z. A. (2026). Oxidative stress and the response of bacteria to it. In *Microbial stress survival* (pp. 217–238). Academic Press. https://doi.org/10.1016/b978-0-443-27622-4.00024-9.

Gan, R.-Y., Lui, W.-Y., Wu, K., Chan, C.-L., Dai, S.-H., Sui, Z.-Q., & Corke, H. (2017). Bioactive compounds and bioactivities of germinated edible seeds and sprouts: An updated review. *Trends in Food Science & Technology, 59*, 1–14. https://doi.org/10.1016/j.tifs.2016.11.010

García, S. N. C., Rodríguez-Herrera, R., Flores, S. N., Silva-Belmares, S. Y., Esparza-González, S. C., Ascacio-Valdés, J. A., & Flores-Gallegos, A. C. (2023). Sprouts as probiotic carriers: A new trend to improve consumer nutrition. *Food Chemistry: Molecular Sciences, 7*, Article 100185. https://doi.org/10.1016/j.fochms.2023.100185

Garner, D., & Kathariou, S. (2016). Fresh produce–associated listeriosis outbreaks, sources of concern, teachable moments, and insights. *Journal of Food Protection, 79*(2), 337–344. https://doi.org/10.4315/0362-028x.jfp-15-387

Generalova, A. N., & Dushina, A. O. (2025). Metal/Metal oxide nanoparticles with antibacterial activity and their potential to disrupt bacterial biofilms: Recent advances with emphasis on the underlying mechanisms. *Advances in Colloid and Interface Science.* , Article 103626. https://doi.org/10.1016/j.cis.2025.103626

Genovese, J., Martins, D. M., Silvetti, T., Brasca, M., Fracassetti, D., Borgonovo, G., Mazzini, S., & Limbo, S. (2025). Development of photo-active chitosan-based films with riboflavin for enhanced antimicrobial food packaging applications. *Molecules, 30*, 4166. https://doi.org/10.3390/molecules30214166

Gilbert, J., Woods, S. M., Turkington, T. K., & Tekauz, A. (2005). Effect of heat treatment to control Fusarium graminearum in wheat seed. *Canadian Journal of Plant Pathology, 27*(3), 448–452. https://doi.org/10.1080/07060660509507244

Hu, Y., Nie, W., Hu, X., & Li, Z. (2016). Microbial decontamination of wheat grain with superheated steam. *Food Control, 62*, 264–269. https://doi.org/10.1016/j.foodcont.2015.11.001

Ikram, A., Saeed, F., Afzaal, M., Imran, A., Niaz, B., Tufail, T., … Anjum, F. M. (2021). Nutritional and end-use perspectives of sprouted grains: A comprehensive review. *Food Science and Nutrition, 9*(8), 4617–4628. https://doi.org/10.1002/fsn3.2408

Janotti, A., & Van de Walle, C. G. (2009). Fundamentals of zinc oxide as a semiconductor. *Reports on Progress in Physics, 72*(12), Article 126501. https://doi.org/10.1088/0034-4885/72/12/126501

Jian, F., Jayas, D. S., & White, N. D. (2013). Can ozone be a new control strategy for pests of stored grain? *Agricultural Research, 2*(1), 1–8. https://doi.org/10.1007/s40003-012-0046-2

Jiang, C., Scholle, F., Jin, F., Wei, Q., Wang, Q., & Ghiladi, R. A. (2024). Chlorophyllin as a photosensitizer in photodynamic antimicrobial materials. *Cellulose, 31*(4), 2475–2491. https://doi.org/10.21203/rs.3.rs-2964210/v1

Jin, S. E., Jin, J. E., Hwang, W., & Hong, S. W. (2019). Photocatalytic antibacterial application of zinc oxide nanoparticles and self-assembled networks under dual UV irradiation for enhanced disinfection. *International Journal of Nanomedicine, 14*, 1737–1751. https://doi.org/10.2147/ijn.s192277

Jin, Z., & Wang, Y. C. (2024). Mitigating fungal contamination of cereals: The efficacy of microplasma-based far-UVC lamps against Aspergillus flavus and Fusarium graminearum. *Food Research International, 190*, Article 114550. https://doi.org/10.1016/j.foodres.2024.114550

Kairyte, K., Kadys, A., & Luksiene, Z. (2013). Antibacterial and antifungal activity of photoactivated ZnO nanoparticles in suspension. *Journal of Photochemistry and Photobiology B: Biology, 128*, 78–84. https://doi.org/10.1016/j.jphotobiol.2013.07.017

Kamel, R. M., El-Kholy, M. M., Tolba, N. M., Amer, A., Eltarawy, A. M., & Ali, L. M. (2022). Influence of germicidal ultraviolet radiation UV-C on the quality of apiaceae spices seeds. *Chemical and Biological Technologies in Agriculture, 9*(1), 89. https://doi.org/10.1186/s40538-022-00358-4

Karabaş, E., Yurddaskal, M., Bozatlı, S. B., & Yılmaz, T. (2025). Production of zinc oxide (ZnO) doped biodegradable film and investigation of its photocatalytic/antimicrobial properties. *Journal of Photochemistry and Photobiology A: Chemistry, 462*, Article 116214. https://doi.org/10.1016/j.jphotochem.2024.116214

Khapre, A. P., Deshpande, H. W., & Katke, S. D. (2020). A review on microbial contamination of cereal grains. *International journal of chemical studies, 8*(3), 1829–1832. https://doi.org/10.22271/chemi.2020.v8.i3y.9474

Kim, I., Viswanathan, K., Kasi, G., Thanakkasaranee, S., Sadeghi, K., & Seo, J. (2020). ZnO nanostructures in active antibacterial food packaging: Preparation methods, antimicrobial mechanisms, safety issues, future prospects, and challenges. *Food Reviews International, 38*(4), 537–565. https://doi.org/10.1080/87559129.2020.1737709

Korkmaz, M., & Polat, M. (2000). Free radical kinetics of irradiated durum wheat. *Radiation Physics and Chemistry, 58*(2), 169–179. https://doi.org/10.1016/s0969-806x(99)00359-x

Kumar, R., Anandan, S., Hembram, K., & Narasinga Rao, T. (2014). Efficient ZnO-based visible-light-driven photocatalyst for antibacterial applications. *ACS Applied Materials and Interfaces, 6*(15), 13138–13148. https://doi.org/10.1021/am502915v

Lai, W., Liu, H., Yan, J., Tian, L., Shi, Y., Xi, Z., & Lin, B. (2025). Photosensitizer of phthalocyanine-conjugated chitosan-doped nano-silver for inactivation against bacteria and promote wound healing. *Biomedical Engineering Advances, 9*, Article 100147. https://doi.org/10.1016/j.bea.2025.100147

Lakshmi Prasanna, V., & Vijayaraghavan, R. (2015). Insight into the mechanism of antibacterial activity of ZnO: Surface defects mediated reactive oxygen species even in the dark. *Langmuir, 31*(33), 9155–9162. https://doi.org/10.1021/acs.langmuir.5b02266

Leanse, L. G., Dos Anjos, C., Mushtaq, S., & Dai, T. (2022). Antimicrobial blue light: A 'magic bullet'for the 21st century and beyond? *Advanced Drug Delivery Reviews, 180*, Article 114057. https://doi.org/10.1016/j.addr.2021.114057

Li, J., Peng, Y., Han, X., Guo, S., Liang, K., & Zhang, M. (2017). Nonlinear optical properties of sodium copper chlorophyllin in aqueous solution. *Journal of Applied Biomaterials & Functional Materials, 15*(1_suppl), 19–24. https://doi.org/10.5301/jabfm.5000350

Li, F., Zhou, L., Cao, J., Wang, Z., Liao, X., & Zhang, Y. (2022). Aggregation induced by the synergy of sodium chloride and high-pressure improves chlorophyll stability. *Food Chemistry, 366*, Article 130577. https://doi.org/10.1016/j.foodchem.2021.130577

Los, A., Ziuzina, D., & Bourke, P. (2018). Current and future technologies for microbiological decontamination of cereal grains. *Journal of Food Science, 83*(6), 1484–1493. https://doi.org/10.1111/1750-3841.14181

Lukseviciute, V., & Luksiene, Z. (2020). Inactivation of molds on the surface of wheat sprouts by chlorophyllin-chitosan coating in the presence of visible LED-based light. *Journal of Photochemistry and Photobiology B: Biology, 202*, Article 111721. https://doi.org/10.1016/j.jphotobiol.2019.111721

Luksiene, Z., & Buchovec, I. (2019). Impact of chlorophyllin-chitosan coating and visible light on the microbial contamination, shelf life, nutritional and visual quality of strawberries. *Innovative Food Science & Emerging Technologies, 52*, 463–472. https://doi.org/10.1016/j.ifset.2019.02.00

Magallanes López, A. M., & Simsek, S. (2021). Pathogens control on wheat and wheat flour: A review. *Cereal Chemistry, 98*(1), 17–30. https://doi.org/10.1002/cche.10345

Mahamuni-Badiger, P., Ghare, V., Nikam, C., et al. (2024). The fungal infections and their inhibition by zinc oxide nanoparticles: An alternative approach to encounter drug resistance. *Nucleus, 67*, 291–309. https://doi.org/10.1007/s13237-023-00439-1

Maldonado-Carmona, N., Ouk, T. S., & Leroy-Lhez, S. (2022). Latest trends on photodynamic disinfection of Gram-negative bacteria: Photosensitizer's structure and delivery systems. *Photochemical and Photobiological Sciences, 21*(1), 113–145. https://doi.org/10.1007/s43630-021-00128-5

Maleki, S., Razavi, S. H., & Yadav, H. (2023). Diabetes and seeds: New horizon to promote human nutrition and anti-diabetics compounds in grains by germination. *Critical Reviews in Food Science and Nutrition, 63*(27), 8457–8477. https://doi.org/10.1080/10408398.2022.2063793

Mendes, C. R., Dilarri, G., Forsan, C. F., Sapata, V. D. M. R., Lopes, P. R. M., de Moraes, P. B., … Bidoia, E. D. (2022). Antibacterial action and target mechanisms of zinc oxide nanoparticles against bacterial pathogens. *Scientific Reports, 12*(1), 2658. https://doi.org/10.21203/rs.3.rs-1054432/v1

Mladenova, R., Solakov, N., Loginovska, K., & Karakirova, Y. (2025). Analysis of gamma-irradiation effect on radicals formation and on antiradical capacity of horse chestnut (Aesculus hippocastanum L.) seeds. *Applied Sciences, 15*(6), 3287. https://doi.org/10.3390/app15063287

Myoda, S. P., Gilbreth, S., Akins-Lewenthal, D., Davidson, S. K., & Samadpour, M. (2019). Occurrence and levels of Salmonella, enterohemorrhagic Escherichia coli, and Listeria in raw wheat. *Journal of Food Protection, 82*(6), 1022–1027. https://doi.org/10.4315/0362-028x.jfp-18-345

Ni, Y., Li, Y., Wang, M., Li, H., Zhang, W., Tan, L., Zhao, J., & Xu, B. (2024). Chitosan-based packaging films with antibacterial-sterilization integrated continuous activity for extending the shelf life of perishable foods. *International Journal of Biological Macromolecules, 275*, Article 133351. https://doi.org/10.1016/j.ijbiomac.2024.133351

Núñez-Salas, R. E., Rodriguez-Chueca, J., Hernández-Ramírez, A., Rodríguez, E., & de Lourdes Maya-Treviño, M. (2021). Evaluation of B-ZnO on photocatalytic inactivation of Escherichia coli and Enterococcus sp. *Journal of Environmental Chemical Engineering, 9*(1), Article 104940. https://doi.org/10.1016/j.jece.2020.104940

Pablos, C., Marugán, J., van Grieken, R., Hamilton, J. W., Ternan, N. G., & Dunlop, P. S. (2024). Assessment of photoactivated chlorophyllin production of singlet oxygen and inactivation of foodborne pathogens. *Catalysts, 14*(8), 507. https://doi.org/10.3390/catal14080507

Polat, M., & Korkmaz, M. (2003). Use of electron spin resonance technique for the detection of irradiated rice seeds (Oryza sativa L.). *International Journal of Food Science and Technology, 38*(6), 653–659. https://doi.org/10.1046/j.1365-2621.2003.00721.x

Popović, V., Fairbanks, N., Pierscianowski, J., Biancaniello, M., Zhou, T., & Koutchma, T. (2018). Feasibility of 3D UV-C treatment to reduce fungal growth and mycotoxin loads on maize and wheat kernels. *Mycotoxin Research, 34*(3), 211–221. https://doi.org/10.1007/s12550-018-0316-3

Puranen, S., Riekkinen, K., & Korhonen, J. (2021). Antibiofilm effects of nanoparticles and visible light illumination against Listeria monocytogenes. *Frontiers in Microbiology, 12*, Article 710954. https://doi.org/10.3389/fmicb.2021.710954

Randhir, R., Kwon, Y. I., & Shetty, K. (2008). Effect of thermal processing on phenolics, antioxidant activity and health-relevant functionality of select grain sprouts and seedlings. *Innovative Food Science & Emerging Technologies, 9*(3), 355–364. https://doi.org/10.1016/j.ifset.2007.10.004

Rezaei, M., Pirsa, S., & Chavoshizadeh, S. (2020). Photocatalytic/antimicrobial active film based on wheat gluten/ZnO nanoparticles. *Journal of Inorganic and Organometallic Polymers and Material, 30*(7), 2654–2665. https://doi.org/10.1007/s10904-019-01407-6

Rizzi, V., Fini, P., Fanelli, F., Placido, T., Semeraro, P., Sibillano, T., … Cosma, P. (2016). Molecular interactions, characterization and photoactivity of Chlorophyll a/chitosan/2-HP-β-cyclodextrin composite films as functional and active surfaces for ROS production. *Food Hydrocolloids, 58*, 98–112. https://doi.org/10.1016/j.foodhyd.2016.02.012

Rose, D. J., Bianchini, A., Martinez, B., & Flores, R. A. (2012). Methods for reducing microbial contamination of wheat flour and effects on functionality. *Cereal Foods World, 57*(3), 104. https://doi.org/10.1094/cfw-57-3-0104

Sanchez, D. R., Jespersen, B. M., Rasmussen, L. H., & Andersen, M. L. (2025). Ozone treatment of wheat reduces common bunt (Tilletia spp.) infection. *Journal of Stored Products Research, 111*, Article 102488. https://doi.org/10.1016/j.jspr.2024.102488

Schmidt, M., Zannini, E., & Arendt, E. K. (2019). Screening of post-harvest decontamination methods for cereal grains and their impact on grain quality and technological performance. *European Food Research and Technology, 245*(5), 1061–1074. https://doi.org/10.1007/s00217-018-3210-5

Shabana, H. A., Mahmoud, T., Gairola, S., Al Ketbi, A., Aljasmi, M., & Al Sallani, M. (2021). Effect of storage conditions and sodium hypochlorite treatment on germination of Cucumis prophetarum (Cucurbitaceae) seeds from arid Arabian deserts. https://doi.org/10.21203/rs.3.rs-201765/v1.

Shrestha, A., & Kishen, A. (2012). Polycationic chitosan-conjugated photosensitizer for antibacterial photodynamic therapy. *Photochemistry and Photobiology, 88*(3), 577–583. https://doi.org/10.1111/j.1751-1097.2011.01026.x

Singh, R., Cheng, S., & Singh, S. (2020). Oxidative stress-mediated genotoxic effect of zinc oxide nanoparticles on Deinococcus radiodurans. *3 Biotech, 10*(2), 66. https://doi.org/10.1007/s13205-020-2054-4

Singh, S., Gade, J. V., Verma, D. K., Elyor, B., & Jain, B. (2024). Exploring ZnO nanoparticles: UV–visible analysis and different size estimation methods. *Optical Materials, 152*, Article 115422. https://doi.org/10.1016/j.optmat.2024.115422

Sirelkhatim, A., Mahmud, S., Seeni, A., et al. (2015). Review on zinc oxide nanoparticles: Antibacterial activity and toxicity mechanism. *Nano-Micro Letters, 7*, 219–242. https://doi.org/10.1007/s40820-015-0040-x

Stankic, S., Suman, S., Haque, F., & Vidic, J. (2016). Pure and multi metal oxide nanoparticles: Synthesis, antibacterial and cytotoxic properties. *Journal of Nanobiotechnology, 14*(1), 73. https://doi.org/10.1186/s12951-016-0225-6

Sun, Y., Li, C., & Lee, A. (2025). Sprouted grains as a source of bioactive compounds for modulating insulin resistance. *Applied Sciences, 15*(15), 8574. https://doi.org/10.3390/app15158574

Szczygieł, T., Koziróg, A., & Otlewska, A. (2024). Synthetic and natural antifungal substances in cereal grain protection: A review of bright and dark sides. *Molecules, 29*(16), 3780. https://doi.org/10.3390/molecules29163780

Takhar, V., & Singh, S. (2025). Nanomaterials ROS: A comprehensive review for environmental applications. Environmental science. *Nano, 12*(5), 2516–2550. https://doi.org/10.1039/d5en00049a

Udovicki, B., Stankovic, S., Tomic, N., Djekic, I., Smigic, N., Trifunovic, B. S., … Rajkovic, A. (2022). Evaluation of ultraviolet irradiation effects on Aspergillus flavus and Aflatoxin B1 in maize and peanut using innovative vibrating decontamination equipment. *Food Control, 134*, Article 108691. https://doi.org/10.1016/j.foodcont.2021.108691

Vagena, I. A., Gatou, M. A., Theocharous, G., Pantelis, P., Gazouli, M., Pippa, N., … Lagopati, N. (2024). Functionalized ZnO-based nanocomposites for diverse biological applications: Current trends and future perspectives. *Nanomaterials, 14*(5), 397. https://doi.org/10.3390/nano14050397

Vazirov, R. A., Narkhova, A. A., Vazirova, E. N., & Sokovnin, S. Y. (2023). Electron paramagnetic resonance signal in wheat seeds irradiated with low-energy electron beam. *Radiation Physics and Chemistry, 208*, Article 110934. https://doi.org/10.1016/j.radphyschem.2023.110934

Vejerano, E. P., & Ahn, J. (2023). Leaves are a source of biogenic persistent free radicals. *Environmental Science and Technology Letters, 10*(8), 662–667. https://doi.org/10.1021/acs.estlett.3c00277

Victória, H. F., Ferreira, D. C., José Filho, B. G., Martins, D. C., Pinheiro, M. V., de Am Sáfar, G., & Krambrock, K. (2022). Detection of singlet oxygen by EPR: The instability of the nitroxyl radicals. *Free Radical Biology and Medicine, 180*, 143–152. https://doi.org/10.1016/j.freeradbiomed.2021.12.303

Vitasovic, T., Caniglia, G., Eghtesadi, N., Ceccato, M., Bojesen, E. D., Gosewinkel, U., … Ferapontova, E. E. (2024). Antibacterial action of Zn2+ ions driven by the in vivo formed ZnO nanoparticles. *ACS Applied Materials & Interfaces, 16*(24), 30847–30859. https://doi.org/10.1021/acsami.4c04682

Wainwright, M., Maisch, T., Nonell, S., et al. (2017). Photoantimicrobials—Are we afraid of the light? *The Lancet Infectious Diseases, 17*(2), e49–e55. https://doi.org/10.1016/S1473-3099(16)30268-7

Wang, W., Li, G., Xia, D., An, T., Zhao, H., & Wong, P. K. (2017). Photocatalytic nanomaterials for solar-driven bacterial inactivation: Recent progress and challenges. Environmental science. *Nano, 4*(4), 782–799. https://doi.org/10.1039/c7en00063d

Wang, F., Wang, R., Pan, Y., Du, M., Zhao, Y., & Liu, H. (2022). Gelatin/chitosan films incorporated with curcumin based on photodynamic inactivation technology for antibacterial food packaging. *Polymers, 14*, 1600. https://doi.org/10.3390/polym14081600

Yang, G., Xu, J., Xu, Y., Guan, X., Ramaswamy, H. S., Lyng, J. G., … Wang, S. (2024). Recent developments in applications of physical fields for microbial decontamination and enhancing nutritional properties of germinated edible seeds and sprouts: A review. *Critical Reviews in Food Science and Nutrition, 64*(33), 12638–12669. https://doi.org/10.1080/10408398.2023.2255671

Yang, H., Zhang, J., Li, Z., Huang, J., Wu, J., Zhang, Y., … Zhao, Y. (2023). Antibacterial effect of low-concentration ZnO nanoparticles on sulfate-reducing bacteria under visible light. *Nanomaterials, 13*(14), 2033. https://doi.org/10.3390/nano13142033

Yang, G., Zhou, D., Hu, D., Fan, L., Li, R., & Wang, S. (2025). Development of potential processing technologies for germinated edible seeds and their applications in food: A comprehensive review. *Critical Reviews in Food Science and Nutrition, 65*(33), 8592–8623. https://doi.org/10.1080/10408398.2025.2505237

Yi, Z., Shan, Z., Fang, L., Lu, C., & Xu, Z. (2023). Enhanced photostability of chlorophyll by introducing Mg2Si as an O2-depleting agent. *Journal of Materials Science, 58*(14), 6281–6296. https://doi.org/10.1007/s10853-023-08398-3

Yılmaz Tuncel, N., Polat Kaya, H., Sakarya, F. B., Andaç, A. E., Korkmaz, F., Ozkan, G., … Capanoglu, E. (2025). The effect of germination on antinutritional components, in vitro starch and protein digestibility, content, and bioaccessibility of phenolics and antioxidants of some Pulses. *Food Science and Nutrition, 13*(5), Article e70103. https://doi.org/10.1002/fsn3.70103

Youf, R., Müller, M., Balasini, A., Thétiot, F., Müller, M., Hascoët, A., … Le Gall, T. (2021). Antimicrobial photodynamic therapy: Latest developments with a focus on combinatory strategies. *Pharmaceutics, 13*(12), 1995. https://doi.org/10.3390/pharmaceutics13121995

Zare, M., Namratha, K., Ilyas, S., Sultana, A., Hezam, A., Sunil, L., Surmeneva, M. A., Surmenev, R. A., Nayan, M. B., Ramakrishna, S., Mathur, S., & Byrappa, K. (2022). Emerging trends for ZnO nanoparticles and their applications in food packaging. *ACS Food Science & Technology, 2*(5), 763–781. https://doi.org/10.1021/acsfoodscitech.2c00043

Zhao, L., Zhou, Y., Yue, W., Duan, D., Liu, R., Yang, L., … Bian, H. (2025). Photodynamic inactivation using natural pigments: dual-ROS mechanisms, delivery strategies, and applications in food preservation. *Lebensmittel-Wissenschaft & Technologie*. , Article 118617. https://doi.org/10.1016/j.lwt.2025.118617

Zhou, T., Yin, Y., Cai, W., Wang, H., Fan, L., He, G., Zhang, J., Jiang, M., & Liu, J. (2021). A new antibacterial nano-system based on hematoporphyrin-carboxymethyl chitosan conjugate for enhanced photostability and photodynamic activity. *Carbohydrate Polymers, 269*, Article 118242. https://doi.org/10.1016/j.carbpol.2021.118242